Large amplitude oscillatory shear of pseudoplastic and elastoviscoplastic materials

Randy H. Ewoldt[1], Peter Winter[1], Jason Maxey[2], and Gareth H. McKinley[1,*]
[1]Hatsopoulos Microfluids Laboratory, Department of Mechanical Engineering, Massachusetts Institute of Technology, Cambridge, MA
[2]Halliburton, Houston, TX

*author to whom correspondence should be addressed, gareth@mit.edu

Abstract

We explore the utility of strain-controlled large amplitude oscillatory shear (LAOS) deformation for identifying and characterizing apparent yield stress responses in elastoviscoplastic materials. Our approach emphasizes the visual representation of the LAOS stress response within the framework of Lissajous curves with strain, strain-rate, and stress as the coordinate axes, in conjunction with quantitative analysis of the corresponding limit cycle behavior. This approach enables us to explore how the material properties characterizing the yielding response depend on both strain amplitude and frequency of deformation. Canonical constitutive models (including the purely viscous Carreau model and the elastic Bingham model) are used to illustrate the characteristic features of pseudoplastic and elastoplastic material responses under large amplitude oscillatory shear. A new parameter, the perfect plastic dissipation ratio, is introduced for uniquely identifying plastic behavior. Experimental results are presented for two complex fluids, a pseudoplastic shear-thinning xanthan gum solution and an elastoviscoplastic invert-emulsion drilling fluid. The LAOS test protocols and the associated material measures provide a rheological fingerprint of the yielding behavior of a complex fluid that can be compactly represented within the domain of a Pipkin diagram defined by the amplitude and timescale of deformation.

Keywords: Nonlinear viscoelasticity - yield stress ï viscoplastic - LAOS ï Lissajous-Bowditch curve

1. Introduction

In this work we examine the response of "yield stress fluids" to large amplitude oscillatory shear (LAOS) deformation. Without seeking to be drawn into an extended debate, we use the term "yield stress fluid" pragmatically to refer to any material or model which exhibits a dramatic change in viscosity (orders of magnitude) over a small range of applied stress (Barnes and Walters (1985); Barnes (1999)). This definition might include pseudoplastic (dramatically shear-thinning) liquids, or elastoviscoplastic [1] materials which effectively behave as linear viscoelastic solids for applied stresses below a critical yield stress $\mathring{u}<\mathring{u}_y$, but irreversibly deform and flow as a fluid for applied stress above the yield stress $\mathring{u}>\mathring{u}_y$.

Yield stress behavior is sometimes desired in order to achieve particular performance with complex fluids. For example, oilfield drilling fluids are often formulated to be yield stress fluids to meet the needs of an intermittent drilling process. While drilling ahead, relatively long periods of fluid flow will be interrupted by short periods (usually less than ten minutes) when the fluid is not pumped as pipe connections are made. During non-drilling activities (tripping pipe, running casing, etc.) the drilling fluid may lie stagnant in the hole for hours or even days. During this period, settling of solids can be especially problematic if the fluid does not have sufficient yield structure to support both large and small particulate matter. However, a fluid with an excessive yield stress can also provide problems; for example, if a large stress is required to break the structure and initiate fluid flow in the well annulus, the result is tremendous pressure surges which may fracture the formation and lead to further problems. The balance between minimizing these *swab* and *surge pressures* while maintaining suspension of *weight materials* (high specific gravity solids, primarily barite) and drilled cuttings can be difficult to maintain in fluids that are thixotropic and exhibit a yield stress (Maxey (2007)).

What is needed is a test protocol for characterizing the elastic, viscous, and yielding characteristics of a prototypical mud in the field or in the formulation laboratory. Large amplitude oscillatory shear (LAOS) is a test method which systematically interconnects familiar material measures such as steady flow viscosity $\eta(\dot{\gamma})$, linear viscoelastic moduli $G'(\omega)$ and $G''(\omega)$,

[1] The terms elastic, viscous, and plastic are sometimes used to refer to specific components of constitutive equations, but here the term elastoviscoplastic is used to refer to experimentally measured material responses as described in the text.

as well as nonlinear viscoelastic properties (Dealy and Wissbrun (1990)), allowing for nonlinear viscous and elastic effects to be characterized simultaneously. In strain-controlled LAOS deformation, the imposed strain takes the form $\gamma(t) = \gamma_0 \sin \omega t$, which consequently imposes a phase-shifted strain-rate $\dot{\gamma} = \gamma_0 \omega \cos \omega t$. The resulting oscillatory shear stress $\sigma(t; \omega, \gamma_0)$ is recorded and analyzed. LAOS tests are completely defined by two input parameters, e.g. frequency and amplitude $\{\text{ɤ}, \text{ɔ}_0\}$. These two parameters define an experimental test space in which results can be compactly represented, which is now known as the Pipkin diagram (Pipkin (1972)). The steady flow curve, $\eta(\dot{\gamma}) = \sigma(\dot{\gamma})/\dot{\gamma}$, is recovered in the limit of small frequency, $\omega \to 0$, whereas the familiar measures of linear viscoelasticity, G'(ω) and G"(ω), are recovered in the limit of small strain amplitude, $\gamma_0 \to 0$. Many complex fluids are processed or utilized outside of these limiting regions, e.g. the oilfield drilling fluids discussed above experience large strains and strain-rates on the order of the reciprocal of the characteristic timescales in the material. LAOS offers a systematic methodology for characterizing viscoelastic material responses over the full domain of amplitudes (ɔ_0) and timescales ($1/\text{ɤ}$) of the imposed shearing deformation.

Methods for analyzing LAOS include Lissajous curves (Philippoff (1966); Tee and Dealy (1975)), Fourier transform rheology (e.g. Wilhelm (2002)), Stress decomposition (Cho *et al.* (2005); Ewoldt *et al.* (2008); Yu *et al.* (2009)), computation of viscoelastic moduli (Hyun *et al.* (2002); Ewoldt *et al.* (2008)), decomposition into characteristic waveforms (Klein *et al.* (2007)), and analysis of parameters related to Fourier transform rheology (Debbaut and Burhin (2002); Hyun and Wilhelm (2009)). A unifying framework, or ontology, for LAOS was recently proposed by Ewoldt *et al.* (2008) which introduced a number of physically-meaningful material measures for LAOS tests and identified the inter-relation between some of the different approaches listed above. The physical meaning of some of these measures was highlighted by considering graphically the raw test data in the form of Lissajous-Bowditch curves, which are parametric plots of stress $\sigma(t)$ vs. strain $\gamma(t)$ or strain-rate $\dot{\gamma}(t)$. This inherently visual approach allows for qualitative interpretations of quantitative material measures such as Fourier or Chebyshev coefficients.

Steady state LAOS responses can be visualized as parametric curves in a 3-D space with strain, strain-rate, and stress as the coordinate axes, $\{\gamma(t), \dot{\gamma}(t), \sigma(t)\}$ (Cho *et al.* (2005)). We

use the term ñelastic Lissajous-Bowditch curveò to denote the projection of the oscillatory response curves onto the stress $\sigma(t)$ vs. strain $\gamma(t)$ plane, whereas viscous Lissajous-Bowditch curves denote parametric plots of stress $\sigma(t)$ vs. strain-rate $\dot{\gamma}(t)$. A linear elastic material response, $\sigma = G\gamma$, appears as a straight line on the elastic Lissajous curve of $\sigma(t)$ vs. $\gamma(t)$, or a circle in a suitably scaled plot of σ / G vs. $\dot{\gamma} / \gamma_0 \omega$. In the linear viscoelastic regime, the Lissajous figures are elliptical when the stress response is a sinusoidal function, $\sigma(t) = \sigma_0 \sin(\omega t + \delta)$ and is plotted against $\gamma(t)$ or $\dot{\gamma}(t)$.

A nonlinear viscoelastic response will distort the elliptical shape of a Lissajous curve. Although very small nonlinearities are best identified quantitatively by the presence of higher harmonics in the Fourier response spectrum, moderate and large nonlinearities are easily identified by the non-elliptical distortions induced in the Lissajous curves. Furthermore, Lissajous curves provide a meaningful way to visualize and interpret viscoelastic nonlinearities in general. The particular nonlinear LAOS signature associated with yield stress fluids such as drilling muds can be identified and better understood by first considering representative constitutive models. Here we consider two canonical models: a purely viscous Carreau model and the elastic Bingham plastic model. We determine the signature responses of these yield stress fluid models in LAOS tests and explore suitable measures for quantifying typical yield-like responses for any material in LAOS. We examine the experimental response of two material samples using these measures; a shear-thinning aqueous xanthan gum solution and an elastoviscoplastic oilfield drilling mud. We show that the LAOS protocol can be used to identify regimes within the shear deformation space $\{\gamma_0, \omega\}$ in which a complex material most closely approximates the response of a yield stress fluid.

2. Materials and Methods

2.1 Materials

The aqueous xanthan gum solution (0.2 wt%) was provided by CPKelco, San Diego, CA in solution form. An oilfield drilling fluid was provided by Baker Hughes Drilling Fluids, Houston, TX. The invert emulsion drilling fluid (IEDF) was obtained as a sample from field operations and had a density of 1.53 g/ml. The fluid component of the drilling mud is an invert emulsion with a continuous mineral oil phase surrounding an internal phase of calcium chloride brine

(17%wt, 1.76 molar). The oil/water ratio was 76/24 (by vol). The drilling mud contained high specific gravity solids (barite) at ~15%wt and organophilic clays ~2%wt. Drilled solids, which primarily consist of a mixture of reactive and non-reactive clays, composed greater than 5%wt of the IEDF.

2.2 LAOS protocol

Large amplitude oscillatory shear (LAOS) tests were performed using an ARES-LS displacement controlled rheometer (TA Instruments). A cone-plate geometry was used for the aqueous xanthan gum solution, diameter D = 50 mm, cone angle Ŭ = 0.0402 rad, truncation h = 0.049 mm. Xanthan gum tests were performed at T=22ºC.

For the drilling fluid, a plate-plate geometry was selected (diameter D = 25 mm, gap h = 0.5 mm) because of the presence of a significant particulate phase. Adhesive-backed, waterproof sandpaper (600 grit) was attached to both the top and bottom plates to inhibit slip at the surface. In an attempt to avoid edge fracture artifacts, the gap was deliberately over-filled with the fluid sample. An outer ring (D=30 mm) was used to contain the over-filled sample. The ring was sealed to the bottom sandpaper surface using vacuum grease. Using a Peltier plate, the temperature of the drilling fluid was maintained at 48.9ºC (i.e. 120ºF which is recommended as standard practice by the American Petroleum Institute (A.P.I. (2009)).

The strain field for the rotational parallel plate geometry is inhomogeneous, and angular displacement and torque are the naturally measured quantities. For the intrinsic variables of strain and stress, we report (and use in subsequent analysis) the strain at the edge of the plate, γ_R, and the apparent stress which would exist at the edge of the plate assuming a linear response, $\sigma_A = 2M/\pi R^3$. The possible artifacts of this approach are given more detailed consideration in a subsequent section below.

Raw data was collected with the native rheometer control software (TA Orchestrator) using the Arbitrary Waveshape test as described by Ewoldt *et al.* (2008). Although extremely high sample rates and signal-to-noise ratios can be achieved by acquiring and oversampling raw voltage signals from the BNC outputs on the back of the ARES (van Dusschoten and Wilhelm (2001)), we find that the Arbitrary Waveshape test sequence provided by the rheometer software allows for sufficiently high sample rates for our analysis without the requirement of a separate

data acquisition system. Furthermore, the sample stress and strain signals are directly accessible with our protocol, and in contrast to the raw voltage signal, our measured variables available from the native rheometer control software presumably include all of the internal calibration factors of the instrument.

2.3 Data Processing

The raw data exported from the rheometer control software was processed using MATLAB®. The majority of data processing is performed using a freely available LAOS data analysis package, MITlaos (Ewoldt *et al.* (2007)). The MITlaos software is used to determine the Fourier coefficients, Chebyshev coefficients, elastic/viscous stress decomposition, and the corresponding viscoelastic moduli. For a specified pair of LAOS input parameters, $\{\gamma, \gamma_0\}$, the sample is subjected to multiple deformation cycles. The initial transient response is monitored and allowed to decay so that a steady-state limit cycle is reached. Six complete strain cycles in the periodic steady state regime are used for the data processing. MITlaos uses the higher-harmonic information, up to a user-specified cutoff harmonic $n_{max} = \omega_{max} / \omega$, to calculate the desired viscoelastic material parameters. For the drilling fluid, the cutoff frequency was chosen to be n_{max}=11 or higher depending on the noise floor of the power spectrum, in order to capture of all the meaningful information in the response signal while avoiding noise. For the xanthan gum solution the cutoff frequency was chosen to be n_{max}=9, except for the lowest frequency test at $\{\gamma$=0.15 rad.s^{-1}, γ_0=1.0$\}$ in which n_{max}=5 was used to filter unnecessary noise in the (small) torque signal. Fig. 1 shows an example of a full time series response of a drilling fluid LAOS test, along with the associated Lissajous curve and normalized harmonic spectrums. The noise floor appears near a normalized intensity of $I_n / I_1 \approx 5 \cdot 10^{-4}$ (Fig. 1b). This noise floor could be reduced by oversampling but would not significantly change the quantitative measurements of the odd harmonics through n=11. Even harmonics are negligible, e.g. $I_2 / I_1 = 2.6 \cdot 10^{-3}$, and do not appear as distinct peaks in the power spectrum.

In order to validate the procedure of using MITlaos to analyze raw stress and strain waveforms we first compared the results from a pair of strain sweep tests performed using the ARES software. One test used the Arbitrary Waveshape protocol with offline processing by MITlaos, and the other test used the standard oscillation protocol of the ARES software, which

does not capture the raw waveforms. The results from these duplicate tests are shown in Fig. 2 for the xanthan gum solution at ω =3.75 rad.s^{-1} and increasing values of strain amplitude γ_0. Good correspondence between the two protocols is obtained for both $G_1'(\omega,\gamma_0)$ and $G_1''(\omega,\gamma_0)$ across the full range of strain amplitudes.

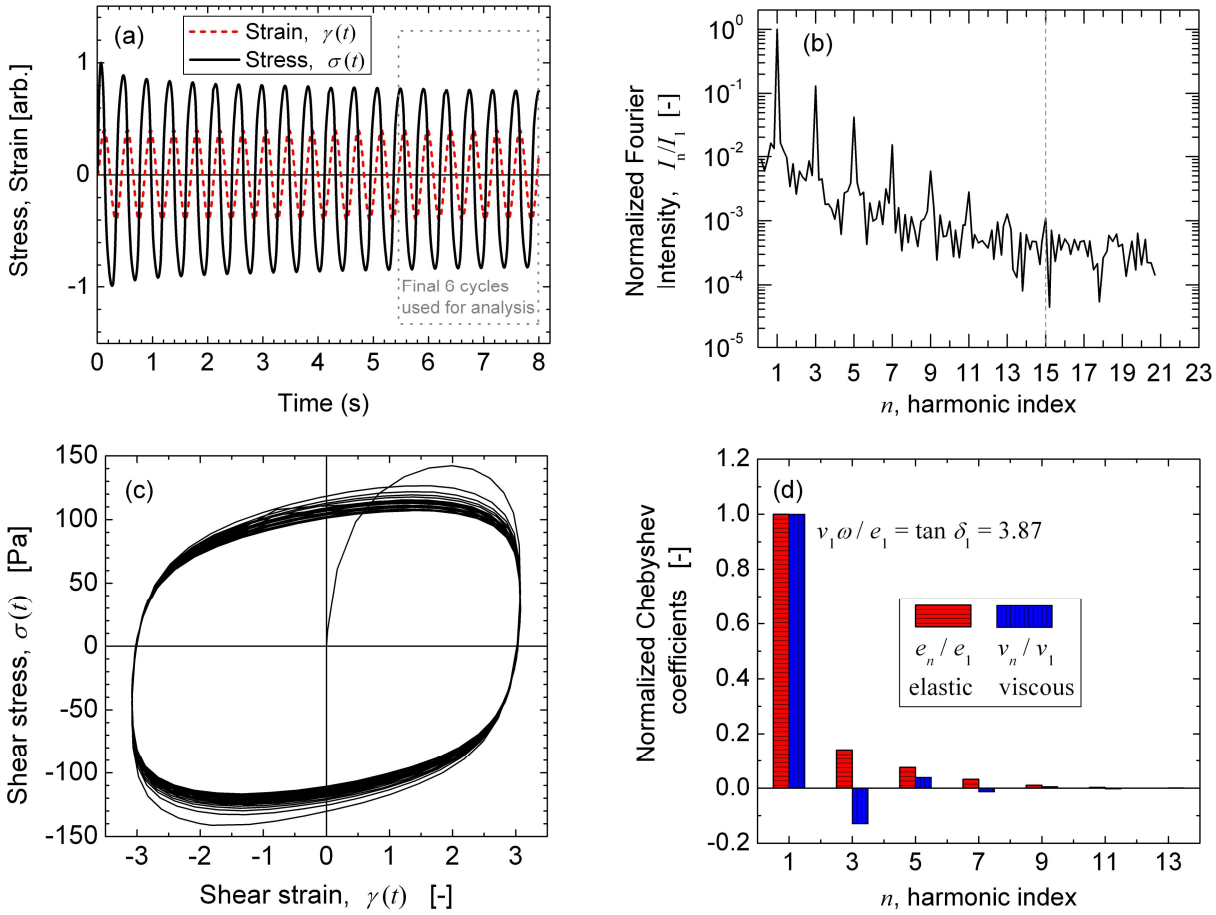

Fig. 1. Data processing example, LAOS of the drilling fluid at $\omega = 15$ rad.s^{-1}, $\gamma_0 = 3.16$. (a) Full time series waveforms of the raw data signals, of which the final six cycles are used for analysis of periodic steady-state oscillations. (b) Normalized power spectrum of the steady oscillatory stress signal. Here a cut-off harmonic n=15 is used for the calculation of viscoelastic parameters. (c) Full waveform shown as a Lissajous curve of stress $\sigma(t)$ vs. strain $\gamma(t)$, and (d) the spectrum of Chebyshev coefficients which decompose the elastic and viscous nonlinearities from the steady oscillatory signal, here $v_1\omega/e_1 = \tan\delta = 3.87$ which indicates that the viscous component is dominant.

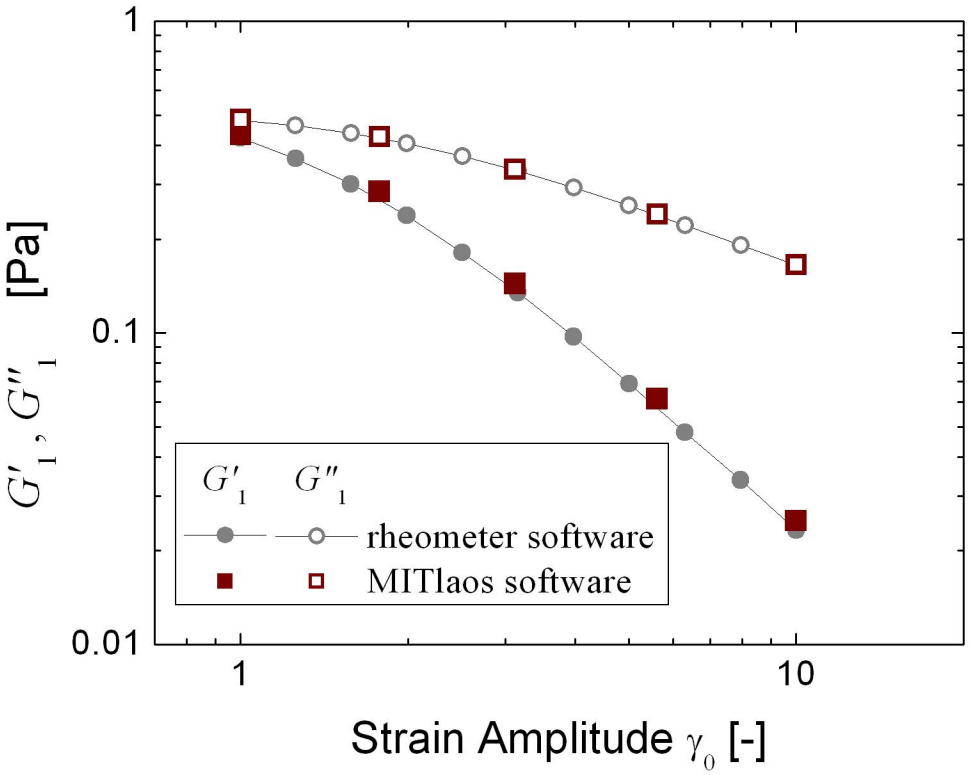

Fig. 2. Validation of the MITlaos software, using a strain sweep for xanthan gum solution (0.2 wt%) at $\dot{\gamma}$ =3.75 rad.s^{-1}. MITlaos software is used to analyze the raw stress and strain waveforms resulting from Arbitrary Waveshape tests (squares). A duplicate test was performed with the typical oscillation test mode of the ARES rheometer software (circles), which provides viscoelastic parameters but no raw data or assessment of higher harmonic content. The superposition of results indicates the validity of the Arbitrary Waveshape test and the MITlaos software for analyzing both linear and nonlinear LAOS results.

3. Response of model fluids with yield stress characteristics

Before we examine experimental LAOS measurements, it is instructive to explore the characteristic features of Lissajous curves for model yield stress fluids. This helps build intuition when examining results from experiments or other proposed constitutive models. Here we consider two models which are simpler limits of a general elastoviscoplastic response. One model is a purely-viscous Generalized Newtonian Fluid which exhibits pseudoplasticity (shear-thinning) and can approach perfect plastic behavior (i.e. a stress response independent of deformation rate) in a specific limit. The second model behaves as a linear elastic solid before

yield with a rate dependent stress after yield. Each model can be allowed to approach the canonical Bingham plastic constitutive response in an appropriate limit.

3.1 Purely viscous Carreau model

Many Generalized Newtonian Fluid models can approach the familiar Bingham plastic limit, for example the Cross model (Cross (1965)), Papanastasiou model (Papanastasiou (1987)), and Carreau-Yasuda model (Bird *et al.* (1987)). Bird *et al.* (1983) and Mitsoulis (2007) provide comprehensive reviews of the relative merits of many of these different models and their utility in solving flow problems. Here we select the Carreau model because of its familiarity and its ability to describe pseudoplastic (shear-thinning) data as well as materials with a critical plastic stress. Furthermore, the model requires only two variables to fully describe a response to LAOS deformation, as shown below.

The Carreau-Yasuda model is a Generalized Newtonian Fluid which describes a non-Newtonian viscosity $\eta(\dot{\gamma})$ as an instantaneous single-valued function of shear rate (Bird *et al.* (1987)). The non-Newtonian viscosity is given as

$$\frac{\eta-\eta_\infty}{\eta_0-\eta_\infty}=\left(1+\left(\lambda\dot{\gamma}\right)^a\right)^{\frac{n-1}{a}} \tag{1}$$

where η_0 is the low-rate Newtonian plateau viscosity, η_∞ is the high-rate plateau viscosity, λ is a characteristic timescale (or more accurately the inverse of a characteristic shear-rate, $\lambda=1/\dot{\gamma}^*$) beyond which non-Newtonian behavior becomes important, n is the power-law exponent, and a is correlated with the sharpness (concavity) of the transition from Newtonian to power-law behavior. Many good fits can be found for a = 2 and $\eta_\infty=0$, especially for polymer solutions and melts (Bird *et al.* (1987)). For a = 2, the model reduces to the Carreau model.

The Carreau model reduces to the Newtonian fluid for n = 1 and describes shear-thinning for n < 1. For n Ÿ 0, and η_0 □ η_∞, the model represents a yield stress fluid in which the viscosity dramatically changes within a small range of stress. The apparent yield stress of the Carreau model (Eq.(1)) for n = 0 can be found by considering the power-law regime, $\lambda\dot{\gamma}$ □ 1, and determining the shear stress from $\sigma=\eta(\dot{\gamma})\dot{\gamma}$. The apparent shear yield stress is found to be $\sigma_Y=\eta_0/\lambda$ in the limit n=0. The Carreau model gives a purely viscous response, because stress

only depends on the instantaneous value of the shear-rate, $\sigma(\dot{\gamma})$. The elastic modulus G' is therefore always zero, even in the nonlinear regime.

The LAOS material response of the Carreau model (Eq.(1), a = 2) can be concisely represented by two parameters when we set $\eta_\infty = 0$ for simplicity. For $x(t) = \gamma(t)/\gamma_0 = \sin\omega t$, $y(t) = \dot{\gamma}(t)/\dot{\gamma}_0 = \cos\omega t$ the dimensionless stress response is

$$\bar{\sigma}(t; n, Cu) = y(t)\left(1 + \left(Cu\ y(t)\right)^2\right)^{\frac{n-1}{2}} \tag{2}$$

where $\bar{\sigma} \equiv \sigma/\eta_0\dot{\gamma}_0$ and $Cu \equiv \lambda\gamma_0\omega$ is the Carreau number. The normalized stress waveform is therefore a function of two non-dimensional parameters. The stress response of Eq.(2) is represented in terms of a family of Lissajous-Bowditch plots in Fig. 3. Fig. 3a depicts the 3D response curve of the normalized stress response as a function of the two orthogonal LAOS inputs, $\sigma(\gamma(t), \dot{\gamma}(t))$. When suitably scaled so that $x(t) = \sin\omega t$ and $y(t) = \cos\omega t$, the periodic system output corresponds to trajectories on the surface of the bounding cylinder shown in gray (Fig. 3a). In the limit n = 1, the response corresponds to a plane curve sectioned through the cylinder with $\sigma_{max} = \eta_0\dot{\gamma}_0$. As n is decreased, the trajectory becomes increasingly distorted and the maximum stress decreases.

The Carreau model approaches a yield stress fluid response as $n \to 0$ and the Carreau number $Cu = \lambda\gamma_0\omega \gg 1$. For this yield stress response, the maximum stress becomes $\sigma_{max} \to \eta_0/\lambda$ and the trajectory approaches two plane semicircles (Fig. 3a, top) offset by $2\sigma_{max} = 2\eta_0/\lambda$. For this yield-like response, normalized elastic Lissajous-Bowditch curves of stress vs. strain appear as squares (Fig. 3a, bottom-left, n=0). The viscous Lissajous-Bowditch curves of stress vs. strain-rate enclose no area and are single-valued functions of the instantaneous strain-rate $y(t) = \dot{\gamma}(t)/\dot{\gamma}_0$ (see Eq.(2)) as expected for all Generalized Newtonian Fluid constitutive models. For this purely viscous response, the slope of any local secant line equals the viscosity, $\eta \equiv \sigma(\dot{\gamma})/\dot{\gamma}$. Near $|\dot{\gamma}| \to 0$ it is the tangent line of the viscous Lissajous curve which represents the low-rate Newtonian plateau viscosity, η_0; however, this becomes increasingly difficult to resolve. The apparent viscosity at the minimum resolvable rate, $\eta'_M \equiv d\sigma/d\dot{\gamma}\big|_{\dot{\gamma}=0}$, and at the largest imposed rate, $\eta'_L \equiv \sigma/\dot{\gamma}\big|_{\dot{\gamma}=\dot{\gamma}_0}$, are two useful measures of the

nonlinear response which are generally applicable to any viscoelastic LAOS response, as discussed by Ewoldt *et al.* (2008).

The limiting yield stress behavior of the Carreau model is representative of a viscoplastic yield stress response. A corresponding elastoplastic limit is considered in the following section.

3.2 Elastic Bingham model – homogeneous strain

The elastic Bingham model responds as a linear elastic solid below the yield stress and transitions to a Bingham plastic response above the yield stress in which recoverable elastic strain is stored during flow (Yoshimura and Prudhomme (1987)). This model incorporates material elasticity below yield and in this sense represents a more general yield stress response than the Carreau model presented in the previous section. This model has recently been used by (Rouyer *et al.* (2008)) to understand the LAOS response of aqueous foams. A number of more general elastoviscoplastic models have also been proposed in the literature (see for example Mujumdar *et al.* (2002), Saramito (2007)); however for simplicity we focus here on the canonical elastoplastic model.

The shear stress-strain relationships for the elastic Bingham model are described by

$$\begin{aligned} \sigma &= G\gamma^E & \left|\gamma^E\right| &< \gamma_Y \\ \sigma &= G\gamma_Y + \mu_p\dot{\gamma} & \left|\gamma^E\right| &= \gamma_Y \end{aligned} \tag{3}$$

where G is the elastic modulus, γ^E is the recoverable elastic strain, γ_Y is the yield strain, and μ_p is the plastic viscosity. The yield stress for this model is $\sigma_Y = G\gamma_Y$. The elastic strain γ^E is found by integrating the shear-rate with respect to time, but saturates at $|\gamma^E| = \gamma_Y$ during flow. When the flow stops and reverses direction, the accumulated elastic strain is recovered and the response is linear elastic until the material is re-yielded again, when $\gamma^E = \pm\gamma_Y$.

(a) $\sigma(t)/\sigma_{max}$ at $\lambda\gamma_0\omega = 10$

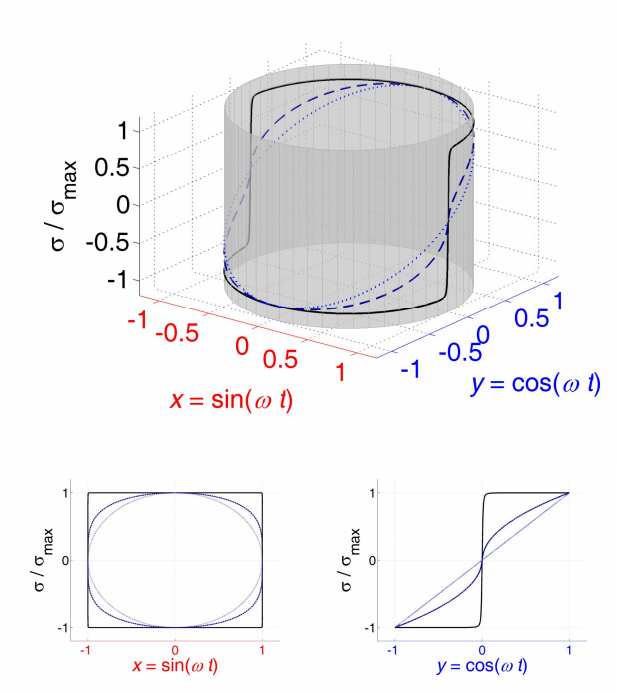

(b) $\sigma(t)/\eta_0\dot{\gamma}_0$ at various $\lambda\gamma_0\omega$

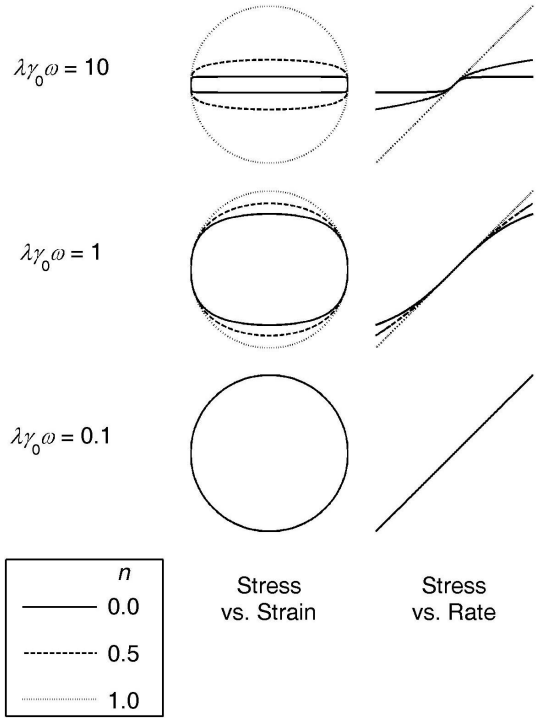

Fig. 3. Lissajous-Bowditch curves of the Carreau pseudoplastic model (Eq.(2)) for various values of the Carreau number $Cu = \lambda\gamma_0\omega$ and power law index n. Here n=1.0 is Newtonian (dotted lines), n=0.5 is shear-thinning (dashed lines), and n=0.0 is the limiting case of viscoplastic yield stress behavior (solid lines). (a) 3D trajectories of the stress response $\sigma(t)/\sigma_{max}$ as a function of the normalized LAOS inputs $\{x(t), y(t)\}$, shown for $\lambda\gamma_0\omega = 10$. Note that the maximum stress σ_{max} is different for each value of n, as shown in (b), which depicts 2D Lissajous curves projected onto the planes of stress vs. strain ($\sigma(t)$ vs. $x(t)$) and stress vs. strain-rate ($\sigma(t)$ vs. $y(t)$). In (b) the stress is scaled by the Newtonian stress $\eta_0\dot{\gamma}_0$, rather than the maximum stress, at each value of the Carreau number $Cu = \lambda\gamma_0\omega$.

The response of the model to LAOS flow is completely governed by two non-dimensional parameters, representing the normalized strain amplitude and normalized strain-rate amplitude (Yoshimura and Prudhomme (1987)),

$$\Gamma_0 = \frac{\gamma_0}{\gamma_Y} \sim \frac{\text{maximum imposed strain}}{\text{yield strain}}$$
$$N = \frac{\mu_p \dot{\gamma}_0}{\sigma_Y} \sim \frac{\text{max viscous stress}}{\text{yield stress}}. \qquad (4)$$

N is related to the inverse of the characteristic Bingham number for LAOS, $N = 1/Bi$ (Bird *et al.* (1983)). Here we use N to parameterize the flow since it directly corresponds to an input of the LAOS deformation, strain-rate amplitude $\dot{\gamma}_0$.

The elastic Bingham model is simulated in homogeneous LAOS flow to produce the Lissajous curves shown in Fig. 4a. For ease of comparison, each Lissajous curve is normalized once again by the maximum stress which is shown above each trajectory. The curves are arranged across the two-dimensional parameter space of strain-rate-amplitude and strain-amplitude (N, $\tilde{u}_0$), which represents the appropriate Pipkin space for the elastic Bingham model response.

The elastic Bingham model reduces to a traditional Bingham plastic as the yield strain goes to zero, $\gamma_Y \to 0$, which corresponds to large values of Γ_0 and the top of the Pipkin space in Fig. 4a. In this viscoplastic limit the stress is only a function of strain rate, $\sigma(\dot{\gamma})$, since the yield criteria is satisfied for almost all times.

The elastic Bingham model further reduces to a perfect plastic model with a constant flow stress after yield as $\mu_p \to 0$, corresponding to $N \to 0$ and $\Gamma_0 \gg 1$ (the top left corner of the Pipkin space of Fig. 4a). In this limit the constitutive equation of the perfect plastic model is written as $\sigma = \sigma_Y \,\mathrm{sgn}(\dot{\gamma})$.

The most prominent feature of the yielded response ($\Gamma_0 > 1$) is a rectangular elastic Lissajous curve, which is approached exactly in the limit of the perfect plastic response ($N \to 0$ at $\Gamma_0 \gg 1$). The elastic Lissajous curve of the perfect plastic response has vertical sides ($G \to \infty$) and a flat top and bottom ($\mu_p \to 0$). The limit of a Bingham plastic model ($\Gamma_0 \gg 1$, arbitrary N) also has vertical sides, but is rounded on the top and bottom because the flow stress is proportional to shear-rate, $\sigma(t) = \sigma_Y + \mu_p \dot{\gamma}(t)$. The full elastoplastic Bingham model response includes an

additional feature, sloped sides, which are caused by the finite elasticity, $d\sigma / d\gamma = G$, for stresses below the yield stress.

For completeness, the *viscous* representation of the Lissajous curves are also shown in Fig. 4a. For the viscous Lissajous curves of stress vs strain-rate, $\sigma(t)$ vs. $\dot{\gamma}(t)$, the importance of the plastic viscosity μ_p term in flow is indicated by the slope of linear portions of the curves (for $\Gamma_0 > 1$). The enclosed area in the center of the viscous Lissajous curves is indicative of the finite elasticity below yield. Elasticity is negligible at $\Gamma_0 \ll 1$, which corresponds to the limit of the (purely viscous) traditional Bingham plastic response. The response is approximately Newtonian in the limit of $\Gamma_0 \ll 1$, $N \gg 1$ (upper-right portion of the Pipkin diagram). In this limit the flow stress dominates, rendering the yield stress negligible. Even though the underlying constitutive model is elastoplastic, the yielding behavior is insignificant for shear deformations at $\Gamma_0 \ll 1, N \gg 1$, and in this part of the deformation space, the LAOS behavior of a material that is described by the elastoplastic Bingham model would instead appear almost Newtonian.

3.3 Elastic Bingham model – torsional plate-plate response

Because of the high volume fraction of solid particulates in many elastoviscoplastic materials such as the drilling fluid considered in the present work, it is typically necessary to use a parallel plate configuration in which the shearing deformation is inhomogeneous. It is therefore necessary to address the possible Lissajous curve artifacts which are introduced by inhomogeneous torsional shear flow. Exploring LAOS plate-plate artifacts is important because this geometry is often used for materials which are susceptible to wall slip and the parallel disk surfaces are easily modified to increase the roughness (e.g. with adhesive-backed sandpaper as used in this work for the drilling fluid). LAOS plate-plate artifacts have been considered in terms of both the harmonic response (Macsporran and Spiers (1982); Macsporran and Spiers (1984)) and the oscillatory response in the time domain (Yoshimura and Prudhomme (1987)). Approximate shift factors have also been considered for matching FT-rheology parameters from cone-plate and parallel plate tests (Wilhelm *et al.* (1999)). Our work here is concerned specifically with Lissajous curves, and we therefore examine the parallel disk artifacts introduced in the form of the Lissajous curves for the elastic Bingham model. The elastic Bingham model (Eq.(3)) under torsional shearing is simulated in the plate-plate geometry

following the same procedure as Yoshimura and Prudhomme (1987). Yield begins at the plate edge for sufficiently large angular displacements, and the radial location of the yield surface separating the yielded and un-yielded regions is time dependent. For the plate-plate geometry, the non-dimensional parameters governing the LAOS torque response involve the relative magnitude of the yield strain γ_Y and the strain amplitude at the edge of the plate, given by $\gamma_0 = \theta_0 R/h$, where R is the plate radius, h is the gap and θ_0 is the maximum angular displacement of the plate. The inhomogeneous strain torque response for the elastic Bingham model is shown in Fig. 4b.

Comparing the plate-plate responses of Fig. 4b with the homogeneous (e.g. cone-plate) responses of Fig. 4a, we observe that the plate-plate artifacts are small, and there is little qualitative difference in the general shapes of Lissajous curves for cone-plate vs. plate-plate deformations with this model. In general, the inhomogeneous kinematics of the plate-plate geometry tend to smooth the linear-to-nonlinear transitions, for instance by rounding some otherwise sharp corners, but otherwise do not introduce any qualitative new features. The strong similarities between the Lissajous curves for cone-plate and plate-plate can be rationalized as follows. First, the range of strain within a plate-plate geometry always varies from $\gamma = 0$ at the center of rotation to $\gamma = \gamma_0$ at the edge of the fixture. Although the strain amplitude at the edge of the plate may transition into the nonlinear regime, e.g. the yielded regime $\Gamma_0 > 1$, part of the sample will always be in the linear regime at sufficiently small radial position *r*. Any dramatic linear-to-nonlinear transition will first occur at the outer edge of the plate, while the majority of the sample remains in the linear elastic (un-yielded) regime. The torque response of any purely strain-dependent transition will therefore be smoothed in LAOS tests with the plate-plate geometry.

Second, the measured torque *M* is weighted by the magnitude of the stress at large radius *r* (i.e. the shear stress in the yielded region). A torque balance between the applied torque and sample stress (neglecting inertia) gives $M = 2\pi \int_0^R \sigma(r) r^2 dr$. The material first yields at the maximum radius $r = R$, and the nonlinear constitutive response will quickly dominate the torque response for the plate-plate geometry. The characteristic shapes of the nonlinear Lissajous curves for the plate-plate and cone-plate flows thus closely resemble each other.

We can quantitatively compare the maximum values of the normalized curves, by examining the peak value of normalized stress shown above each curve, $\left(\sigma/\sigma_Y\right)_{\max}$. For the cone-plate geometry this value approaches $\left(\sigma/\sigma_Y\right)_{\max} \to 1$ in the yielded region ($\Gamma_0 > 1$) and at low strain-rate amplitudes (N<1). For the plate-plate response, the peak value of the normalized torque $\left(2M/\pi R^3\sigma_Y\right)_{\max}$ is shown above each curve, or equivalently $\left(\sigma_A/\sigma_Y\right)_{\max}$ where $\sigma_A = 2M/\pi R^3$ is the apparent stress which would exist at $r = R$ for a linear material response at a given torque M (this corresponds to the typical method of estimating the stress at the plate edge based on a torque measurement (Bird *et al.* (1987))). In the yielded region at low strain-rate amplitude (N<1), we observe from Fig. 4b that $\left(\sigma_A/\sigma_Y\right)_{\max} \to 4/3$. That is, the assumed edge stress is larger than the actual model yield stress by only 33% (Brunn and Asoud (2002)). This numerical value 4/3 can be understood by determining the torque response M for a perfect plastic material in which the shear stress is constant throughout the sample with magnitude $\sigma(r) = \sigma_Y$. Substituting into the normalized torque expression gives

$$\left(\frac{2M}{\pi R^3\sigma_Y}\right)_{\max} = \frac{2}{\pi R^3\sigma_Y}\frac{2\pi R^3\sigma_Y}{3} = \frac{4}{3}. \qquad (5)$$

Note that the plate-plate results in the yielded region for high strain-rates ($N \geq 1$, upper-right of the Pipkin space, Fig. 4b) are also slight overestimates of the actual maximum stress (compare to Fig. 4a), but the difference is smaller in this region. The difference between cone-plate and plate-plate is smaller here because the material response for $\Gamma_0 > 1$, $N \geq 1$, becomes dominated by the plastic viscosity term, which is inherently a linear response in this model.

This analysis provides a broad interpretation of the artifacts in Lissajous curves that can be expected to be introduced from LAOS tests in a parallel plate rheometer. In general, the inhomogeneous strain field softens the nonlinear features of the response and leads to small overestimation of stresses for shear-thinning or yield stress materials. The preceding analysis will aid in the interpretation of the LAOS response for the drilling fluid examined in this work, and also for future LAOS tests using parallel plate fixtures.

Elastic Curves
(load vs. deformation)

Viscous Curves
(load vs. deformation-rate)

(a) homogeneous strain

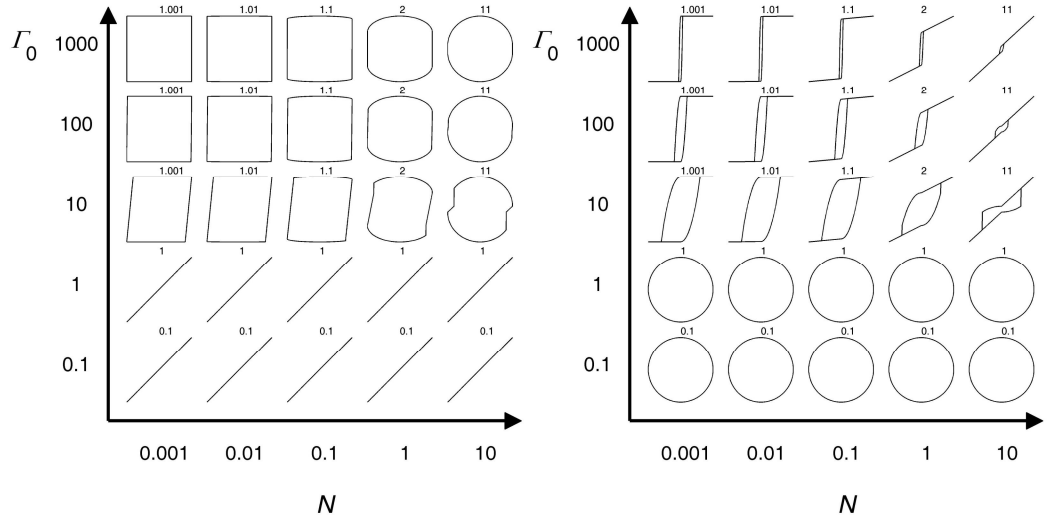

(b) plate-plate

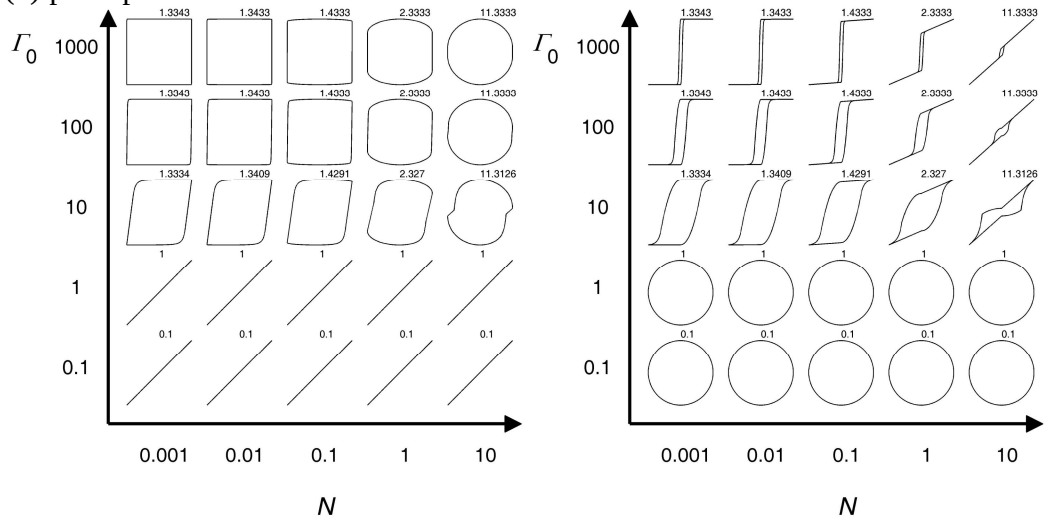

Fig. 4 Lissajous-Bowditch curves for the elastic Bingham model in terms of the variables $\Gamma_0 = \gamma_0 / \gamma_Y$, $N = \mu_p \dot{\gamma}_0 / \sigma_Y$ defined by Yoshimura and Prudhomme (1987). All curves are two-dimensional projections of fully three-dimensional Lissajous curves, $\sigma(\gamma(t), \dot{\gamma}(t))$. (a) Homogeneous strain (e.g. cone-plate) response showing individual limit cycles of the oscillatory stress vs. strain (elastic curves) and stress vs. strain-rate (viscous curves). Maximum normalized stress $(\sigma / \sigma_Y)_{\max}$ is shown above each curve. (b) Steady oscillatory response of plate-plate deformation (inhomogeneous strain), curves of torque vs. displacement (elastic curves) and torque vs. displacement-rate (viscous curves). The maximum normalized torque shown above each curve, $\left(2M / \pi R^3 \sigma_Y\right)_{\max}$.

4. Quantitative indicators of plastic behavior in LAOS

The rheological response of a complex fluid in LAOS can be characterized by numerous material parameters, including strain- and frequency-dependent viscoelastic moduli and higher-harmonic coefficients Wilhelm (2002). In this section we consider the expected behavior of such viscoelastic parameters for a yield stress fluid in response to large amplitude deformation. We also introduce a measure that we refer to as the perfect plastic dissipation ratio, ϕ, which acts as a metric for quantifying how closely a particular LAOS response is to the perfect plastic response of an idealized yield stress fluid.

4.1. Harmonic analysis and Chebyshev coefficients

For strain-controlled LAOS, $\gamma(t) = \gamma_0 \sin \omega t$, the stress response can be represented in the time domain by a Fourier series (Dealy and Wissbrun (1990)) of the form

$$\sigma\left(t;\omega,\gamma_0\right) = \gamma_0 \sum_n \left\{ G_n'\left(\omega,\gamma_0\right) \sin n\omega t + G_n''\left(\omega,\gamma_0\right) \cos n\omega t \right\}. \tag{6}$$

On the basis of symmetry arguments it can be shown that the series contains only odd harmonics (*n*: odd) for typical rheological behavior in which the material response only changes sign if the coordinate system is reversed, i.e. where $\sigma(x,y) = -\sigma(-x,-y)$ (Cho *et al.* (2005)). Such symmetry corresponds to Lissajous curves which can be rotated by 180 degrees about an axis normal to a coordinate plane and retake the same shape. This precludes the presence of even harmonic terms in Eq.(6). Even harmonic terms can be observed in responses which are periodic but do not have 180 degree rotational symmetry, in transient rheological responses (e.g. when the oscillatory waveforms are not strictly periodic and do not close), in the presence of secondary flows (Atalik and Keunings (2004)), or in flows with dynamic wall slip events (Graham (1995)) due to the existence of transient events.

Even harmonics have been discussed as possible indicators of wall slip or yield stress (Harris and Bogie (1967); Macsporran and Spiers (1984); Fischer *et al.* (2007); Klein *et al.* (2007)). However, the presence of even harmonics does *not* specifically indicate a wall slip or yield stress material response in general, nor does the absence of even harmonics indicate the lack of wall

slip. For example, Yoshimura and Prudhomme (1988) examined the LAOS response of a simple slip layer at the surface of a linear viscoelastic model and did not observe even harmonics. Even-harmonics are only related to *non-periodic* or *asymmetric* slip/yield responses. Any stress response which is steady, periodic, and unchanged if the coordinate system is reversed (e.g. a perfect plastic yield stress) will result in only odd, integer harmonics in the Fourier series representation (Eq.(6)).

The harmonic material coefficients in Eq.(6) have a characteristic form for fluids exhibiting idealized yield stress behavior. As we have shown, the ideal perfect plastic yield stress response appears as a square wave in the time domain, $\sigma(t) = \sigma_Y \,\mathrm{sgn}(\dot{\gamma}(t))$. The spectrum of Fourier coefficients for this square wave behavior is

$$\begin{aligned} G_n' &= 0 \\ G_n'' &= \frac{4}{\pi}\frac{\sigma_Y}{\gamma_o}\frac{1}{n}(-1)^{\frac{n-1}{2}} \qquad n:\text{odd} \end{aligned} \tag{7}$$

which indicates that the higher order viscous Fourier coefficients decay as 1/*n* (Klein *et al.* (2007)). The third-harmonic Fourier coefficients have recently been given a physical meaning through the use of Chebyshev polynomial analysis (Ewoldt *et al.* (2008)). The signs of the third-order Chebyshev coefficients, $e_3 = -G_3'$ and $v_3 = G_3''/\omega$, indicate how the nonlinear contributions to the elastic and viscous stresses evolve. For the perfect plastic, $e_3 = 0$ which confirms the absence of elastic contributions to the stress and $v_3 = -4\sigma_Y/3\pi\dot{\gamma}_0$ is negative and therefore correctly indicates shear-thinning. Although the single parameter v_3 correctly indicates that a plastic-like material is strongly shear-thinning, it is not *per se* a sensitive discriminator of a yield stress response. Other materials including pseudoplastic liquids will give rise to negative values of v_3. More specifically, it is the scaling in the decay of the higher viscous harmonics, $v_n \sim 1/\gamma_0 \omega n$, rather than the value of a single coefficient, which indicates a Lissajous curve approaching the perfect plastic yield stress response limit associated with the rectangular shape shown in Fig. 4a.

4.2. Viscoelastic moduli

The presence of a critical stress or yield stress intrinsically leads to nonlinear behavior, and we therefore consider more general LAOS measures which quantify material nonlinearity within a periodic limit cycle (i.e. a single closed Lissajous curve). Ewoldt *et al.* (2008) introduced several dimensionless indexes of nonlinearity which can be applied broadly to any complex fluid response and which approach limiting values for idealized yield stress behavior. These indexes depend on local definitions of the elastic modulus and dynamic viscosity within a single periodic LAOS cycle. The elastic modulus at the minimum resolvable strain G'_M, and the largest imposed strain G'_L, respectively, are given by

$$G'_M \equiv \left.\frac{d\sigma}{d\gamma}\right|_{\gamma=0} = e_1 - 3e_3 + \ldots, \qquad G'_L \equiv \left.\frac{\sigma}{\gamma}\right|_{\gamma=\gamma_0} = e_1 + e_3 + \ldots \tag{8}$$

The apparent viscosity at the minimum resolvable shear rate and the largest imposed shear rate, respectively, are given by:

$$\eta'_M \equiv \left.\frac{d\sigma}{d\dot{\gamma}}\right|_{\dot{\gamma}=0} = v_1 - 3v_3 + \ldots, \qquad \eta'_L \equiv \left.\frac{\sigma}{\dot{\gamma}}\right|_{\dot{\gamma}=\dot{\gamma}_0} = v_1 + v_3 + \ldots \tag{9}$$

These measures (Eqs.(8),(9)) make use of the Lissajous curves to provide a physically meaningful interpretation of each parameter, and for a linear viscoelastic response the definitions reduce identically to G' and η', respectively (Ewoldt *et al.* (2008)). The dimensionless indexes of nonlinearity compare the elastic moduli (or dynamic viscosities) at large and minimum strain (or strain-rate), according to

$$S \equiv \frac{G'_L - G'_M}{G'_L} = \frac{4e_3 - 4e_5 + \ldots}{e_1 + e_3 + e_5 + \ldots}, \qquad T \equiv \frac{\eta'_L - \eta'_M}{\eta'_L} = \frac{4v_3 - 4v_5 + \ldots}{v_1 + v_3 + v_5 + \ldots} \tag{10}$$

in which nonlinearities are indicated by non-zero values, and the nature of nonlinearity is captured by the signs of the strain-stiffening index *S* and shear-thickening index *T*.

We first discuss the limiting value of the strain-stiffening measure *S*. For an idealized perfect plastic model ($\sigma = \sigma_Y \,\mathrm{sgn}(\dot{\gamma})$) or any Generalized Newtonian Fluid model (i.e. solely shear-rate dependent such as the Carreau model), $G'_M = 0$ and $G'_L = 0$, thus *S*=0/0 and is formally undefined. However, for any real experiment with finite data acquisition rates (or in the limiting case of the elastic Bingham model approaching a perfect plastic), $G'_M = 0$ and $G'_L \approx \sigma_Y/\gamma_0 = \text{finite}$. Thus in

the limit of a perfect plastic response ($\Gamma_0 \gg 1$, $N \to 0$ corresponding to the upper-left region of Fig. 4a), we expect $S = \left(G'_L - 0\right)/G'_L \to 1$.

The limiting value of the shear-thickening coefficient T is also undefined for the perfect plastic model. The large-rate dynamic viscosity is readily determined to be $\eta'_L = \sigma_Y/\dot{\gamma}_0$, but the minimum-rate viscosity is undefined due to the discontinuous analytical response at $\dot{\gamma} = 0$. We therefore consider the apparent minimum-rate dynamic viscosity which would be determined from the finite data acquisition rate (or the spacing of simulated data). In fact, η'_M diverges as the resolution of the shear-rate increases, and thus represents the dynamic viscosity at the *minimum* strain-rate which can be resolved by the number of data points available. In such a case η'_M will be finite but very large, $\eta'_M \gg \eta'_L$. We find that T is then a function of data-acquisition rate, which is undesirable in a material measure. As sampling rate of a given experiment improves (or for the elastic Bingham model in the limit of $\Gamma_0 \gg 1$, $N \gg 1$), the value of T would behave as $T = \left(\eta'_L - \eta'_M\right)/\eta'_L \approx -\eta'_M/\eta'_L \to -\infty$ for a perfect plastic. The value of T evaluated for the Carreau model (Fig. 3) also depends on the sampling rate. With sufficiently fine data spacing, $\eta'_M \to \eta_0$; in this limit $T = \left(\eta'_L - \eta'_M\right)/\eta'_L \approx -\eta_0/\eta(\dot{\gamma}_0) = -\left(1 + Cu^2\right)^{\frac{1-n}{2}}$ for the Carreau model.

The nonlinear viscoelastic measures discussed in this section are all well-defined for an arbitrary elastoviscoplastic response. However, for yield stress materials, the parameters systematically approach limiting values which depend on the data acquisition rate (i.e. higher point density creates larger apparent slopes at discontinuities), making it difficult to compare results from different tests. In the following section we propose a material measure which is well-defined and has almost no sensitivity to the data acquisition rate.

4.3. Perfect plastic dissipation ratio

We consider here a scalar metric for quantifying how close a measured material response corresponds to rigid, perfect plastic yield stress behavior ($\sigma = \sigma_Y \operatorname{sgn}(\dot{\gamma})$). Rigid, perfectly plastic behavior is an idealized approximation for a material which exhibits negligible elastic strains in comparison with large plastic deformations at practically constant stress (Ugural and

Fenster (2003)). Physically, this corresponds to a microstructure which can be disrupted by a yield stress, but after disruption incremental deformation is comparatively easy. For example, the stress to deform and disrupt the initial microstructure may be much larger than the incremental stress required to generate additional deformation. Such a response can originate from strong short-range interparticle forces which maintain a jammed or percolated solid phase, but once the solid structure is disrupted the structural units (solid particles, emulsified droplets, etc.) are readily aligned by the flow and the additional contribution of the viscous stress is very small. This behavior is approximately observed for many ñapparent yield stress fluidsò such as colloidal suspensions, microgel pastes, and dense emulsions, as evidenced by nearly constant flow stress over a wide range of shear-rates (see Barnes (1999) for various examples of such stress plateaus).

We compare the energy dissipated in a single LAOS cycle to the energy which would be dissipated in a rigid, perfect plastic response with equivalent strain amplitude γ_0 and maximum stress $\sigma_{\max}$. The perfect plastic response, $\sigma = \sigma_Y \operatorname{sgn}(\dot{\gamma})$, represents the maximum possible dissipated energy for a given strain amplitude γ_0 and maximum stress $\sigma_{\max}$.

The energy dissipated per unit volume in a single LAOS cycle, $E_d = \oint \sigma \, d\gamma$, can be visualized by the area enclosed by the Lissajous curve of stress vs. strain. The Lissajous curve for the corresponding perfect plastic reference response is always a rectangle which circumscribes the measured response on a plot of stress vs. strain. An example is shown in Fig. 5. The energy dissipated per cycle by the perfect plastic in large amplitude oscillatory shear is $\left(E_d\right)_{pp} = \left(2\gamma_0\right)\left(2\sigma_{\max}\right)$. The local shape of a Lissajous curve depends on all of the harmonics, but the total energy dissipated per cycle by any harmonic strain-controlled LAOS response is only a function of the first-order viscous Fourier coefficient (Ganeriwala and Rotz (1987)), and is given by $E_d = \pi \gamma_0^{\,2} G_1''$.

Normalizing the actual dissipated energy by the perfect plastic dissipation gives a dissipation ratio, ϕ, which takes the following values for some simple model responses:

$$\phi \equiv \frac{E_d}{\left(E_d\right)_{pp}} = \frac{\pi \gamma_0 G_1''}{4\sigma_{\max}} \quad \begin{cases} \to 1 & \text{Perfect Plastic} \\ \to \pi/4 = 0.785 & \text{Newtonian} \\ \to 0 & \text{Purely Elastic} \end{cases} \tag{11}$$

This scalar measure is well-behaved for any arbitrary LAOS response, since the strain amplitude and maximum stress are always well-defined and easily determined from the data. This dimensionless measure ϕ can be universally applied to any measured LAOS response, as it compares the unknown response with the maximum possible energy dissipation, which is represented by the perfect plastic model. For a general LAOS response, we expect $\phi = \phi(\gamma_0, G_1'', \sigma_{\max})$. As an example, for a linear viscoelastic response, $\sigma_{\max} = \gamma_0 |G^*|$ and thus $\phi = \frac{\pi G''}{4|G^*|} = \frac{\pi}{4}\sin\delta$. For a more general nonlinear viscoelastic response, $\sigma_{\max} = f(\gamma_0, G_n', G_n'')$ and thus ϕ is a complicated function of the higher-order coefficients.

We can use the constitutive models presented here (the Carreau model and the elastic Bingham model) to guide the interpretation of the perfect plastic dissipation ratio ϕ. For the elastic Bingham model with homogeneous deformation (Fig. 4a), it is clear that $\phi = 0$ in the un-yielded regime $\Gamma_0 \le 1$ (since no energy is dissipated, $E_d = 0$). For $\Gamma_0 > 1$ in the yielded regime, ϕ takes positive values. We have analyzed the response curves in Fig. 4a to calculate the corresponding values of ϕ. At the lowest normalized frequency, $N = 0.001$, the three curves shown at scaled strains of $\Gamma_0 = 10, 100, 1000$ result in dissipation ratios $\phi = 0.900, 0.990, 0.999$. Thus, in the top left corner of the Pipkin space, ($N = 0.001$, $\Gamma_0 = 1000$) the response deviates by only 0.1% from an idealized rigid, perfect plastic response. At the largest normalized frequency shown, $N = 10$, the three curves shown at the scaled strains of $\Gamma_0 = 10, 100, 1000$ result in dissipation ratios $\phi = 0.759, 0.803, 0.805$. These responses are dominated by the viscous flow stress which is linearly dependent on shear-rate, and ϕ is close to the Newtonian fluid reference value, $\phi \approx \pi / 4 \approx 0.785$ in this region of the Pipkin space.

A closed form expression for ϕ can be derived for the Carreau model response to LAOS. Using the definition for ϕ (Eq. (11)), and substituting (Eq.(2)) for the Carreau model stress response, together with the change of variable $d\gamma = \frac{d\gamma}{d(\omega t)} d(\omega t) = \gamma_0 \cos(\omega t) d(\omega t)$, gives

$$\phi_{\text{Carreau}}(n,Cu) = \frac{\oint \sigma(\omega t)d\gamma}{4\sigma_{\max}\gamma_0} = \frac{1}{4}\frac{\int_0^{2\pi} \cos^2\omega t\left(1+\left(Cu\,\cos\omega t\right)^2\right)^{\frac{n-1}{2}} d(\omega t)}{\left(1+\left(Cu\right)^2\right)^{\frac{n-1}{2}}} \tag{12}$$

where the Carreau number is $Cu = \lambda\dot{\gamma}_0 = \lambda\gamma_0\omega$. Fig. 6 shows the behavior of Eq.(12), which will serve as a reference for interpreting ϕ for a predominantly viscous LAOS response. As the power law index $n \to 0$ and the Carreau number $Cu \gg 1$, the value of ϕ smoothly and monotonically approaches the limit $\phi \to 1$. This measure thus gives an unambiguous method of assessing how close a given material response is to that of a perfect plastic under LAOS deformations.

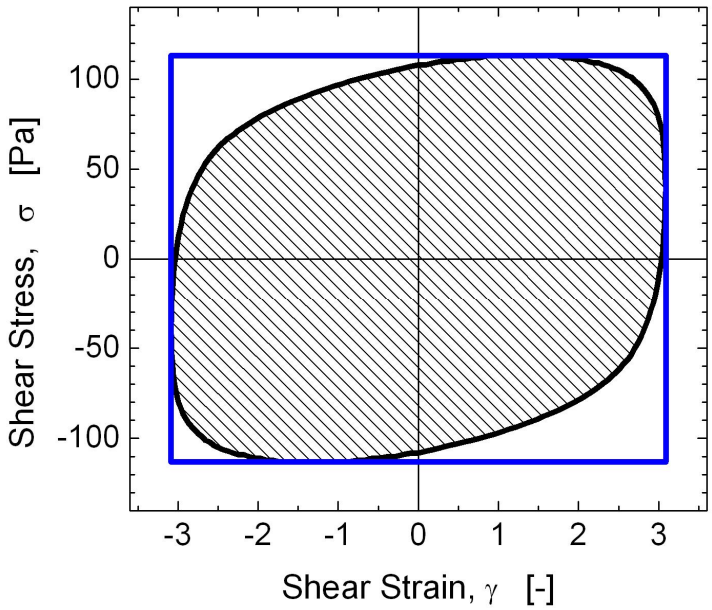

Fig. 5. The energy dissipated by a single LAOS response is represented by the area enclosed in a Lissajous curve of stress vs. strain. For a given strain amplitude γ_0 and maximum stress $\sigma_{\max}$, the maximum possible dissipated energy is the circumscribing rectangle of the perfect plastic model response, with strain amplitude γ_0 and yield stress $\sigma_Y = \sigma_{\max}$. The example shown here is the measured steady LAOS response of the drilling fluid at ω=15 rad.s^{-1}, with $\gamma_0 = 3.16$, $\sigma_{\max} = 113\,\text{Pa}$, and $\phi = 0.829$.

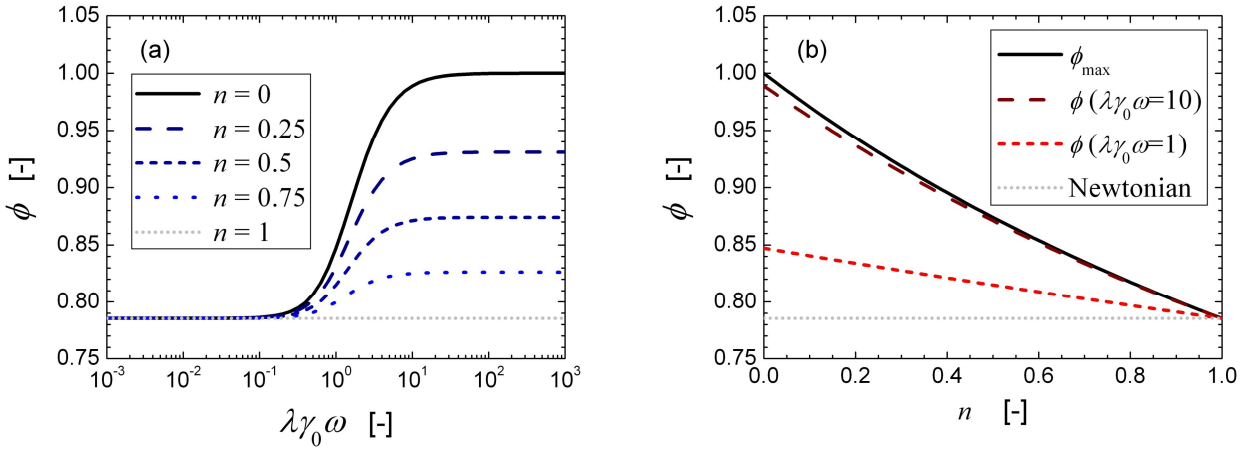

Fig. 6. Carreau model response, characterized by the perfect plastic dissipation ratio, $\phi = \phi(n, \lambda\gamma_0\omega)$ (Eq.(12)). (a) Behavior of ϕ with respect to normalized shear-rate amplitude. (b) Behavior of ϕ as a function of n, shown for various values of the Carreau number $Cu = \lambda\gamma_0\omega$: ϕ_{max}, $\phi(\lambda\gamma_0\omega = 10)$, $\phi(\lambda\gamma_0\omega = 1)$.

5. Experimental Results

In this section we examine experimentally the nonlinear oscillatory response of two fluids, a strongly shear-thinning (pseudoplastic) fluid and an elastoviscoplastic drilling fluild. We use the various material measures introduced above for indicating the yield-like character of the fluid response in LAOS.

Fig. 7 depicts a purely viscous perspective of the fluid characterization, showing flow curves of shear viscosity η for each fluid sample along with fits to the Carreau model of Eq.(1) (for a = 2). For the xanthan gum, a constant shear rate was applied and the steady state value of the viscosity was recorded, after which a higher shear-rate was applied and the process repeated. For the drilling mud, a thixotropic loop test was performed to match experimental conditions for tests on other drilling fluids (Maxey (2007)). The drilling fluid sample was pre-sheared at $\dot{\gamma}_R = 1022$ s^{-1} for 60s (where $\dot{\gamma}_R$ is the shear-rate at the rim of the plate), followed by a 10 minute wait time. The shear-rate was then linearly ramped up from $\dot{\gamma}_R = 0 - 1000$ s^{-1} over 450 seconds, and immediately ramped down, linearly from $\dot{\gamma}_R = 1000 - 0$ s^{-1}. The time between data points limits the minimum resolution of shear-rate to approximately $\Delta\dot{\gamma}_R = 3$ s^{-1}.

Each material exhibits pronounced shear thinning behavior. For the xanthan gum, a Carreau model fit (forcing $\eta_\infty = 0$) results in the parameters $\eta_0 = 1.50$ Pa.s, $\lambda = 8.0$ s, $n = 0.35$ (c.f. Eq.(1)). The power law exponent does not approach yield-like behavior, which would be indicated by $n \to 0$.

In contrast, the drilling fluid is closer to viscoplastic and approaches a yield stress fluid response. The apparent and corrected flow curves for the drilling fluid are shown in Fig. 7 (open symbols are apparent stress, closed symbols show the corrected stress). For steady flow between parallel plates, the true stress can be determined from $\sigma_R = \sigma_A \frac{1}{4}\left(3 + d\ln\sigma_A / d\ln\dot{\gamma}_R\right)$ (e.g. see Macosko (1994)), where σ_R is the true stress at the edge of the disk and σ_A is the apparent stress determined by $\sigma_A = 2M/\pi R^3$ where M is the measured torque and R is the disk radius. Applying this correction requires derivatives of the apparent stress data. To calculate the required derivatives, we fit a fifth order polynomial function to the raw data of $\ln\sigma_A$ vs. $\ln\dot{\gamma}_R$, since this allows calculation of the derivative of an smooth analytical function rather than differentiating discrete raw data. A Carreau fit to the corrected viscosity (filled symbols) of the drilling fluid (allowing for the term η_∞) results in the parameters $\eta_0 = 3.29 \cdot 10^7$ Pa.s, $\lambda = 2.60 \cdot 10^6$ s, $\eta_\infty = 0.337$ Pa.s, and $n = 0.099$. The experimental data lacks a Newtonian plateau in the limit of low shear rates, and therefore the values of η_0 and λ cannot independently be fit with high precision. However, a low value of the rms error is associated with a specific combination of these two parameters in the power-law shear thinning region for which experimental data is available. For $\lambda\dot{\gamma} \gg 1$, $\eta_0 \gg \eta_\infty$, the viscosity is approximately $\eta(\dot{\gamma}) \approx \eta_0(\lambda\dot{\gamma})^{n-1}$ before the approach to the high shear-rate plateau. For the drilling fluid $n = 0.099$, and therefore $\eta_0\lambda^{-0.901} = 55.4$ Pa.s$^{-0.901}$ gives the lowest value of the rms error between the model and the data in the power-law shear-thinning region. Additional rheological tests, which approach the Newtonian plateau in the limit of low shear rate, are required to precisely determine η_0 and λ lambda independently. LAOS tests at low frequencies and large strains (so that the material is yielded) can provide such information and can thus be used to refine the values of the constitutive parameters as we show below.

The strongly shear-thinning nature of the drilling fluid is apparent from the very low power law exponent $n \approx 1$. The yield-like behavior is readily observed by replotting the flow curve in the form of viscosity vs. stress $\eta(\sigma)$ (Fig. 7, inset); the viscosity of the drilling mud changes by more than a factor of ten while the stress changes by less than a factor of two. LAOS tests over a range of frequency and strain amplitude can be used to further explore the behavior of these materials, from linear to nonlinear viscoelastic responses, to reveal how much each material acts like a yield stress fluid for some fraction of the relevant deformation parameter space $\{\gamma, \omega_0\}$.

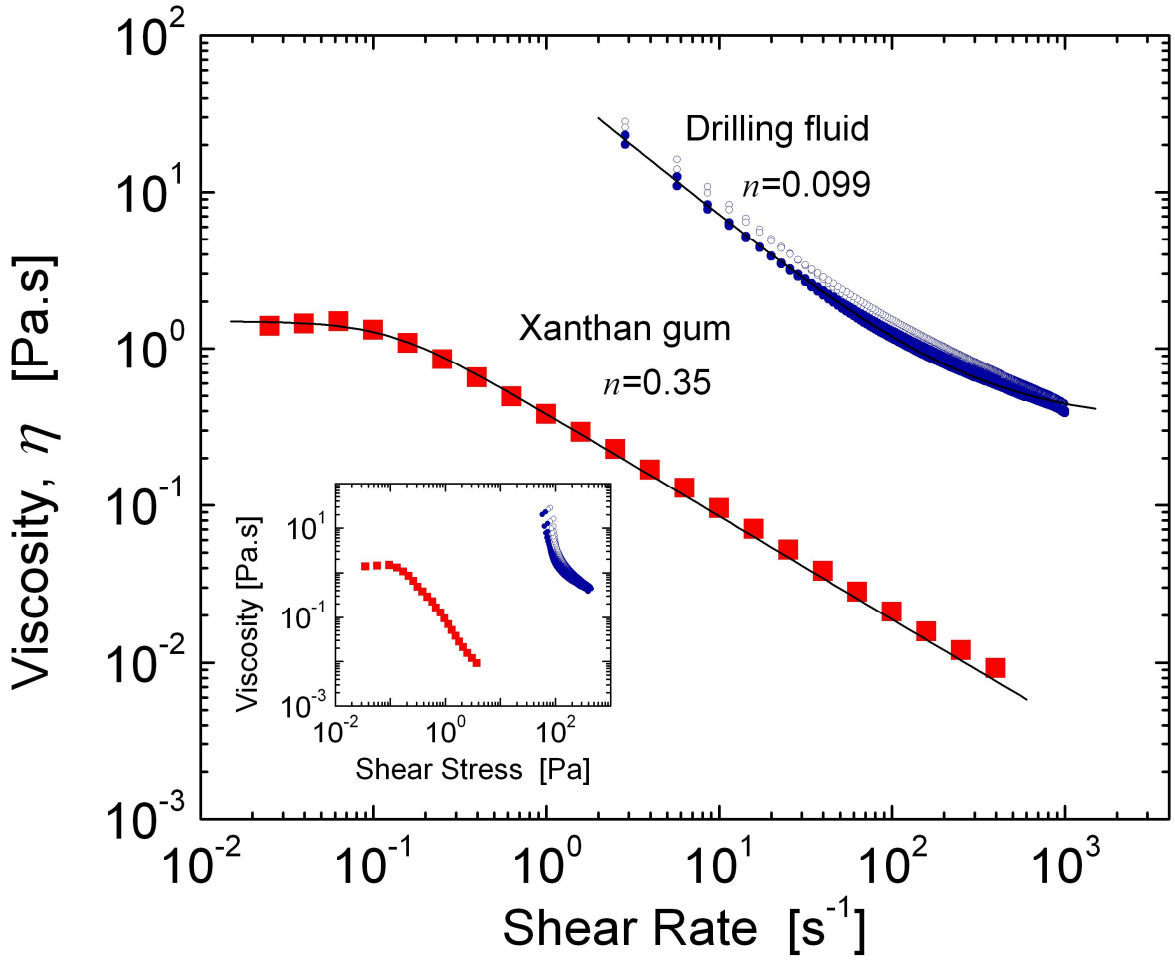

Fig. 7 Viscosity flow curves for the 0.2wt% xanthan gum solution (squares, step shear rate for each data point) and the invert emulsion drilling fluid (thixotropic loop test; open circles depict apparent viscosity and closed circles represent the parallel disk correction). Fits to the Carreau model are shown for each fluid (lines). The inset plot gives viscosity vs. stress.

5.1 Xanthan gum LAOS response

LAOS results for the 0.2% xanthan gum are shown in Fig. 8 (steady state smoothed data), and Fig. 9 (rheological fingerprints of potential yield stress indicators). LAOS tests were performed at four frequencies and five strain amplitudes, which are all shown in Fig. 8. For each frequency and strain amplitude $\{\gamma_0, \omega\}$, the final six steady state cycles are processed to produce the Lissajous curves in Fig. 8. Fig. 8a shows the 3D Lissajous curve traces at ω=3.75 rad.s^{-1}. The full Pipkin space response is shown in Fig. 8b,c, which includes elastic Lissajous curves of the total stress (and the corresponding elastic stress contribution) vs. strain and also viscous Lissajous curves of stress (and viscous stress) vs. strain-rate. The response is linear viscoelastic at all strain amplitudes $\gamma_0 \leq 1$, as shown by the elliptical Lissajous figures and the linear shape of the elastic and viscous stress contributions. The frequency domain $\omega = 0.15 - 18.75$ rad.s^{-1} encompasses a range of phase angle $41^\circ \leq \delta \leq 61^\circ$ (in the linear viscoelastic regime), and therefore includes the G'=G'' crossover frequency at which $\tan\delta = 1$. For strains $\gamma_0 > 1$ the response becomes increasingly nonlinear and pseudoplastic in nature. The onset of non-linearity in the elastic stress and viscous stress functions are quickly identified by visual inspection, and correlate with the distortion of the elliptical shape of the limit cycles showing the periodic variations in the total stress. As the strain-amplitude increases, the curves of total stress vs. strain become increasingly rectangular with strongly rounded corners (consistent with the Carreau model with $0 < n < 1$, c.f.Fig. 3). The Lissajous curves of stress vs. strain-rate (Fig. 8c) appear as shear-thinning at the largest strain amplitude. The response is primarily viscous in the low frequency, large amplitude regime, since the single-valued curves of viscous stress $\sigma''(t)$ vs. strain-rate $\dot{\gamma}(t)$ closely correspond with the loops of total stress $\sigma(t)$ vs. strain-rate $\dot{\gamma}(t)$ (Fig. 8c). The xanthan gum solution is therefore a shear-thinning viscoelastic liquid.

The similarity to a yield-like response can be quantified by examining contour plots of *S*, *T*, and ϕ, as shown in Fig. 9 (other viscoelastic parameters (e_1, e_3, δ, etc.) can be shown as contours in the 2-D space of $\{\gamma_0, \omega\}$, but are omitted here for clarity and brevity). For a perfect plastic response, these parameters are expected to approach the limiting values $S \to 1$, $T \to -\infty$, and $\phi = 1$. Within the limits of the linear regime ($\gamma_0 = 1$), we observe $S \approx 0.05$ and $T \approx 0.05$ indicating an approximately linear viscoelastic response as expected. At low strain amplitude the

perfect plastic dissipation ratio, shown in Fig. 9c, is less than expected for a Newtonian fluid ($\phi < \pi/4$) as expected for a material response that is, in fact, partially elastic (and stores energy).

At larger strain amplitudes, values of S~$O(1)$ indicate strain-stiffening in the elastic response and $T \approx -0.25$ indicates shear-thinning. At these large strains, the plots in Fig. 9b,c indicate a region in which the xanthan gum solution is pseudoplastic in nature ($T < 0, \phi > \pi/4$). However, the maximum observed value, $\phi = 0.87$, does not indicate an idealized yield stress response. This experimentally measured maximum value of $\phi(\omega = 15 \text{ rad.s}^{-1}, \gamma_0 = 10) = 0.87$ is close to (but slightly lower) than predicted by the parameters of the Carreau model fit (Fig. 7, n=0.35, λ=8.0s), which results in $\phi(n = 0.35, Cu = 12) = 0.90$ (c.f. Fig. 6 and Eq.(12)). This suggests that elasticity plays a weak role in this region of the deformation space, which is consistent with the Lissajous curves at (ω=0.15s^{-1}, γ_0=10). The significance of elasticity in the fluid at large Carreau numbers is also indicated by the observed functional dependence of ϕ, shown by the contours in Fig. 9c. For a purely viscous fluid such as the Carreau model, the dissipation ratio is only a function of the shear-rate amplitude, $\phi(\dot{\gamma}_0 = \gamma_0\omega)$. For such a case, ϕ would be constant along lines of constant shear-rate amplitude which correspond to lines with slope -1 on the log-log plot of Fig. 9c. Instead, lines of constant ϕ are approximately horizontal, and ϕ is a strong function of the strain amplitude, $\phi \approx \phi(\gamma_0)$ which indicates the significance of elastic behavior for the range of deformation parameters {ω, γ_0} shown in Fig. 8 and Fig. 9.

Consistent with the inspection of the steady flow curves shown in Fig. 7, the xanthan gum solution is best described as a shear-thinning viscoelastic liquid but without a distinguishable yield stress behavior. We conclude that the dissipation ratio ϕ correctly distinguishes a moderately shear-thinning material response from a yield stress response.

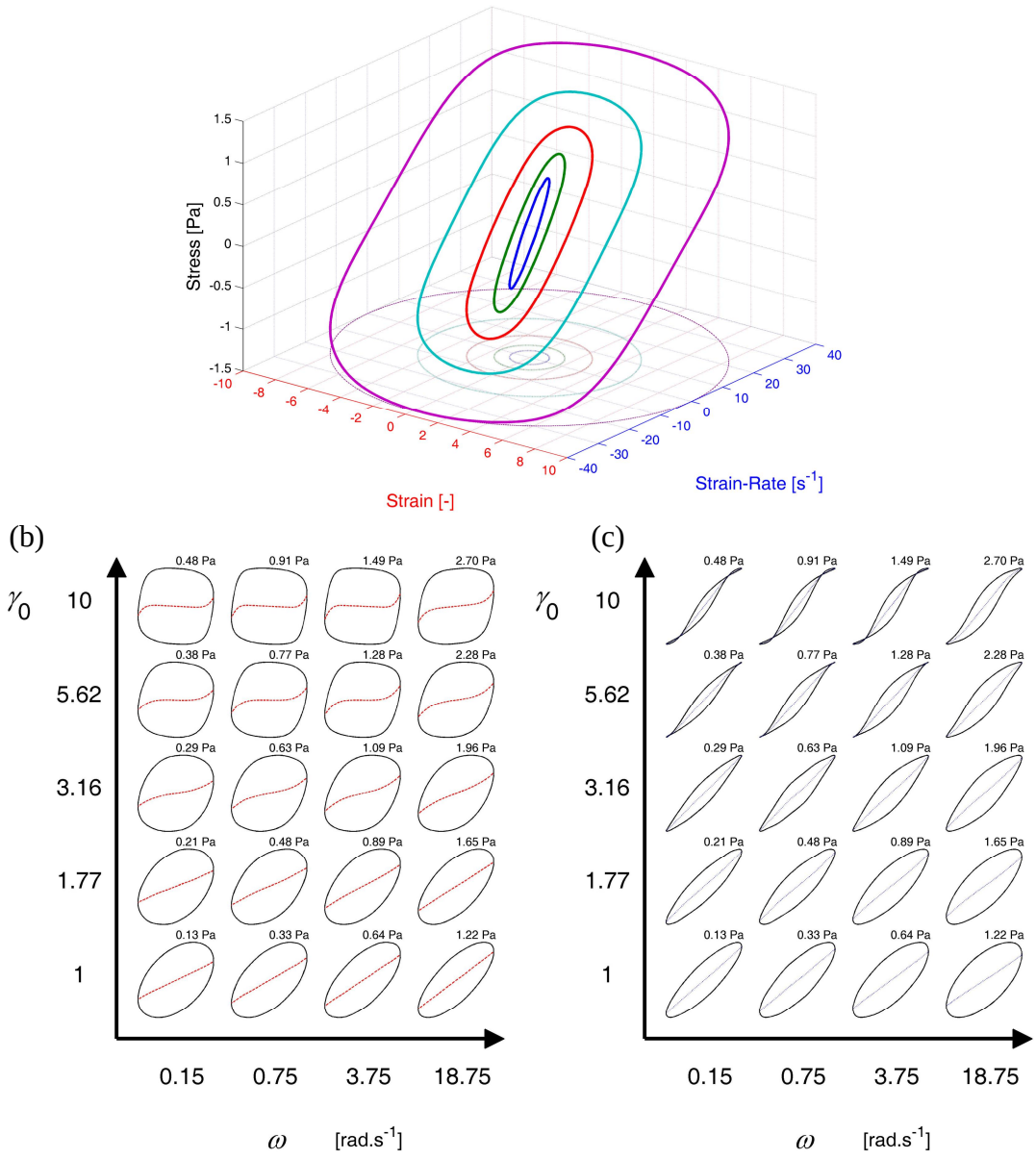

Fig. 8. Steady-state Lissajous curves for the xanthan gum solution (0.2wt% aqueous). (a) Un-normalized 3D Lissajous curves at $\omega = 3.75$ rad.s^{-1}. (b,c) Normalized curves arranged in a Pipkin space at the corresponding input parameters of frequency and strain-amplitude, $\{\gamma, \gamma_0\}$. (b) individual plots of normalized stress (solid black lines) and elastic stress (dashed red lines) vs. strain; (c) individual plots of normalized stress (solid black lines) and viscous stress (dotted blue lines) vs. strain-rate. The maximum stress σ_{max} in each test is shown above each limit cycle.

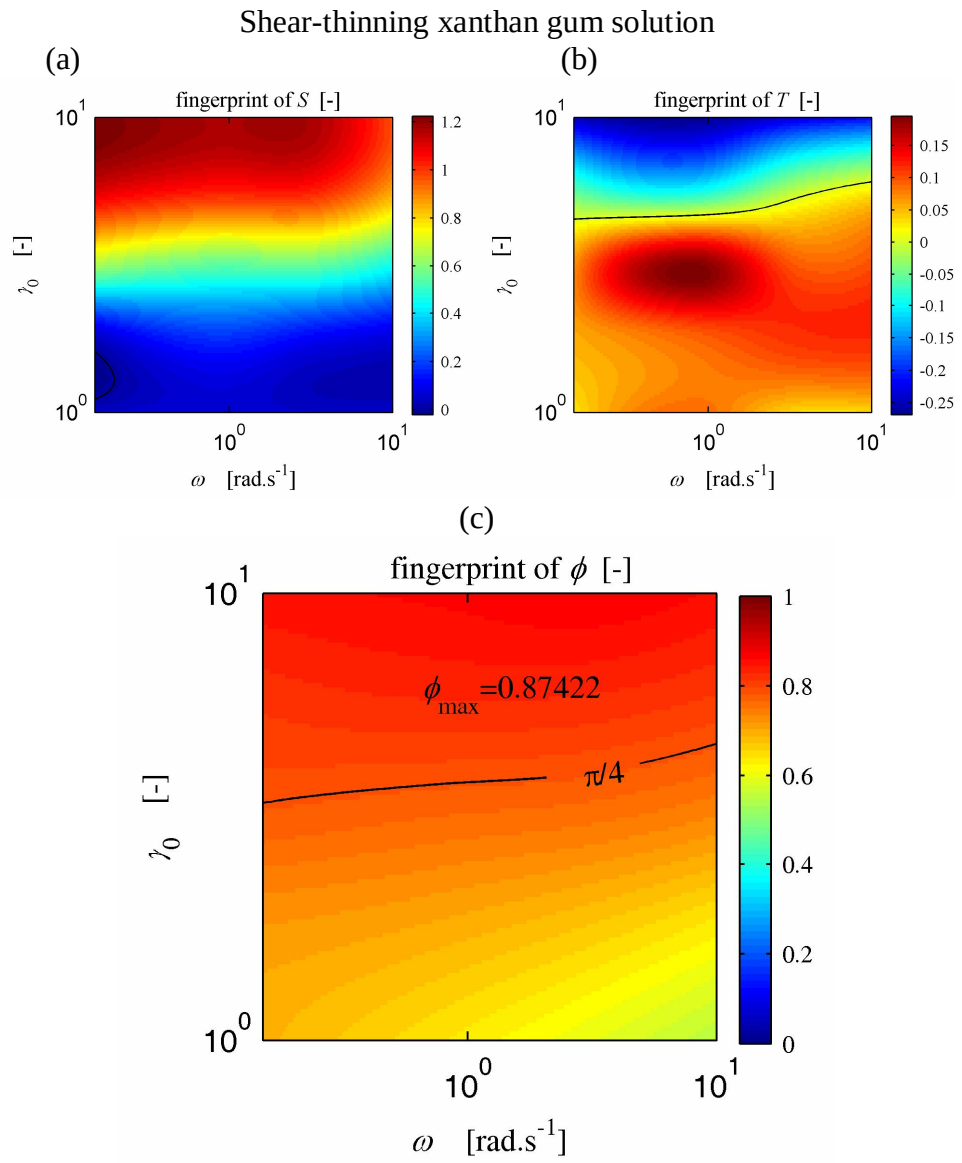

Fig. 9. Yield stress indicators for the xanthan gum solution (0.2wt% aqueous), shown as a function of the LAOS input parameters $\{\gamma_0, \omega\}$. (a,b) Stiffening index and Thickening index, respectively, lines shown at S=0, T=0. (c) perfect plastic dissipation ratio ϕ. $\phi > \pi/4$ indicates a region in which the Xanthan gum solution is shear-thinning. The maximum observed value, $\phi_{max} = 0.87$ at $\{\omega = 3.75$ rad.s$^{-1}, \gamma_0 = 10\}$, does not indicate an idealized yield stress response, which would appear as $\phi_{PP} = 1$.

5.2 Drilling fluid LAOS response

LAOS results for the drilling fluid are shown in Fig. 10 (processed Lissajous curves) and Fig. 11 (rheological fingerprints of yield stress indicators). A predominantly elastic regime can be observed at sufficiently small strain amplitudes. At the minimum imposed strain amplitude, $\gamma_0 = 0.01$, the material response is already weakly nonlinear and viscoelastic as indicated by the nonlinearities in the curves of elastic stress (dashed line) and viscous stress (dotted line) in Fig. 10b,c. It is typical for a filled system to exhibit a nonlinear material response at such small strain amplitude.

As the strain amplitude is increased, the material exhibits a rich nonlinear response in which the elastic stress curves indicate strong elastic strain stiffening for strain amplitude $\gamma_0 \approx 0.1$. The nonlinearity is sufficiently strong that the viscous Lissajous curves appear to self-intersect, forming secondary loops. These apparent self-intersections lead to the formation of secondary loops and are quite generally observed in sufficiently nonlinear LAOS responses. For example, they can also be observed with the xanthan gum solution (Fig. 8c, $\gamma_0 = 10$, $\omega = 0.15 - 3.75$ rad.s^{-1}) and have been observed for other material systems including a micelle solution (Ewoldt *et al.* (2008)), a polystyrene solution (Jeyaseelan and Giacomin (2008)), molten polystyrene (Tee and Dealy (1975)), and a polymer melt in the absence of long-chain branching (Stadler *et al.* (2008)). Some nonlinear viscoelastic constitutive models also show secondary loops, including a non-affine network model (Jeyaseelan and Giacomin (2008)) and a single mode Giesekus model (Ewoldt and McKinley (submitted in concert with this manuscript)). Such secondary loops are correlated with viscoelastic stress overshoots in which the instantaneous stress is unloaded more quickly than new deformation is accumulated (Ewoldt *et al.* (2008)), quantitatively corresponding to negative values of G'_M . A detailed description of this phenomenon is given in a companion communication (Ewoldt and McKinley (submitted in concert with this manuscript)). Animations of three-dimensional space curves (Fig. 8 and Fig. 10) are provided as supporting material. The complexities of this transition regime could not be observed by a steady flow viscosity curve, but are revealed here by the LAOS protocol.

As the deformation amplitude continues to increase ($\gamma_0 \approx 1$), the sample becomes increasingly plastic as indicated by the increasing area enclosed by the elastic Lissajous curves (Fig. 10) and the corresponding increase in the values of the dissipation ratio, ϕ (Fig. 11). However, for

strains $\gamma_0 \approx 1$ none of the Lissajous responses are representative of a perfect plastic material, and moreover the dissipation ratio is smaller than the Newtonian benchmark, $\phi(\gamma_0 = 1) < \phi_{\text{Newtonian}}$. The material is thus properly denoted as elastoplastic in nature.

In order to observe behavior close to perfect plastic, the strain amplitude must be further increased ($\gamma_0 = 10$) so that the sample fully yields. At this amplitude, the drilling fluid visually appears to behave as a viscoplastic fluid (Fig. 10). The shapes of Lissajous curves at $\gamma_0 = 10$ are consistent with the elastic Bingham model (c.f. Fig. 4). Here the Lissajous curves of stress vs. strain become increasingly rectangular in the upper-left of the Pipkin space with additional rounding from viscous stress at high deformation rate amplitudes (upper-right of the Pipkin space).

Fig. 11 shows the rheological fingerprints of the potential discriminators of yield-like behavior, *S*, *T*, and ϕ. As previously discussed, for yield-like behavior, these parameters take the limiting values $S \to 1$, $T \to -\infty$, and $\phi = 1$. In Fig. 11a, the value of *S* approaches *S* = 1 in the upper left of the Pipkin space. At $\gamma_0 = 10$, we measure *S* = 0.94, 1.07, 0.90 at $\dot{\gamma}$ = 0.475, 1.5, 4.75 rad.s^{-1}, respectively. However, the stiffening ratio *S* inherently represents elastic nonlinearities, and therefore also takes the value $S > 1$ at other locations in the Pipkin space over which sufficient strain-stiffening is observed, notably in the region $\gamma_0 \approx 0.1$. Thus, for complex nonlinear viscoelastic material responses, *S*~O(1) is associated with, but does not uniquely identify, a yield-like response.

The shear thickening ratio, *T,* captures intra-cycle viscous nonlinearities. From Fig. 11b, it is clear that *T* does become negative for a yield-like response in the drilling fluid (upper left region of the Pipkin space). However, the most negative values of *T* occur at moderate strain amplitudes, $\gamma_0 \approx 0.1$, and lower frequencies where the drilling fluid response exhibits a strongly nonlinear viscoelastic response (see Fig. 10b,c) but not a yield-like response specifically. We therefore conclude that negative values of *T* may be associated with a strong pseudoplastic response, but local extrema cannot be used to precisely indicate a yield-like response.

In Fig. 11c we investigate the ability of the perfect plastic dissipation ratio to uniquely identify a yield-like response. The value of ϕ is strictly related to the energy dissipated per cycle, rather than other intra-cycle nonlinearities, and is therefore robust to complex nonlinear

viscoelastic responses such that $\phi \to 1$ is uniquely associated with a perfect plastic response. For the drilling fluid, the maximum dissipation ratio is $\phi_{max} \approx 0.93$ which is observed at moderate frequencies and large strains {ϑ =0.475 rad.s^{-1}, ϑ$_0$=10}. The corresponding maximal value of the measured apparent stress at {ϑ =0.475 rad.s^{-1}, ϑ$_0$=10} is $\sigma_{A,\max} = 102\,\text{Pa}$, which is higher than the prediction from the purely viscous Carreau model fit from Fig. 7, in which $\sigma_A = 84\,\text{Pa}$ at $\dot{\gamma} = \dot{\gamma}_0 = 4.75\ \text{s}^{-1}$. This provides a measure of the dynamic yield stress in the fluid at these deformation conditions.

The perfect plastic indicator, ϕ, typically reaches its maximum value for large strain-amplitude γ_0 and low frequency ϑ. This is the case for the viscous and viscoelastoplastic constitutive models as well as the experimental results shown in Fig. 11c. This asymptotic limit $\phi \to 1$ at large strain-amplitude γ_0 and low frequency ϑ can be understood by considering the response of the elastic Bingham model (Fig. 4). For this model, the elastic portion of the yielded response is negligible as $\gamma_0 \gg \gamma_Y$ (creating vertical sides of the Lissajous curves), and the viscous stress is approximately constant for small values of $\dot{\gamma}_0 = \gamma_0\omega$ (corresponding to small values of ϑ at a given γ_0), which creates a flat top to the Lissajous curve. In contrast, for large shear-rate amplitudes $\dot{\gamma}_0$, the elastic Bingham model response is predominantly Newtonian, since the instantaneous rate-dependent plastic viscosity ($\mu_p\dot{\gamma}(t)$) dominates the pre-yield elastic stress ($G\gamma_Y$). Thus, the elastic Bingham model approaches the perfect plastic response in the upper-left corner of the Pipkin space (large amplitude γ_0 and small frequency ϑ), in agreement with the experimental response of the elastoviscoplastic drilling fluid.

Finally, we note that LAOS results can be used to augment the rheological measurements in steady shear (Fig. 7) by providing measurements of the viscous response at progressively lower values of the shear rate $\dot{\gamma}_0 = \gamma_0\omega$. In Fig. 12 we show the agreement between measurements of the apparent steady shear viscosity $\eta(\dot{\gamma})$ (limited to $\dot{\gamma} \geq 1s^{-1}$) and the apparent dynamic viscosity $\nu_1(\dot{\gamma}_0) = \eta_1'(\dot{\gamma}_0)$ for oscillatory shear-rate amplitudes down to $\dot{\gamma}_0 = 3\times10^{-3}s^{-1}$. Good overlap in the data is observed, especially at larger strain amplitudes. This is a manifestation of the so-called Rutgers-Delaware rule (or ǿextended Cox-Merzô rule) for yield stress fluids

Doraiswamy *et al.* (1991). The plateau at the minimum LAOS shear-rate amplitudes is used to determine a lower bound for the Carreau model estimates of η_0 and λ, which could not be independently fitted with any precision from the data in Fig. 7. As previously discussed, the value $\eta_0\lambda^{-0.901} = 55.4\ \text{Pa.s}^{-0.901}$ is required to match the true viscosity of the drilling fluid response in the shear-thinning region. Fig. 12 suggests a lower bound of $\eta_0 \approx 1\times10^3$ Pa.s which corresponds to $\lambda \approx 53$ s. This modified Carreau model fit (for the shear-rate-dependent viscosity) is shown in Fig. 12.

Closer inspection of the data in Fig. 12 shows that as the strain-amplitude is reduced (at fixed frequency) the LAOS data in fact systematically deviate *below* the extrapolated viscous response. This is because the material is not really yielded at these strains. From Fig. 11, it is clear that we need to impose strains $\gamma_0 \geq 3$ to achieve $\phi > \pi/4$, corresponding to a yielded material that is dissipating at least as much energy per cycle as a Newtonian fluid. One of the necessary conditions for the validity of the Rutgers-Delaware rule is ñhigh strain amplitudeò (Mujumdar *et al.* (2002), Doraiswamy *et al.* (1991)), i.e. strain amplitudes much larger than the yield strain. The absolute value of the ñlarge strainò required to successfully apply this rule will be different between materials, but the material measure ϕ helps to unambiguously identify highly-yielded regimes (corresponding to $\phi > \pi/4$) in which the Rutgers-Delaware rule will be most applicable.

6. Conclusions

Large amplitude oscillatory shear (LAOS) deformations provide a rich picture of the yielding transitions in a complex elastoviscoplastic fluid in terms of variations with respect to the strain amplitude and frequency of imposed deformation. This rich behavior can be represented in terms of 3D Lissajous curves $\sigma(\gamma(t),\dot{\gamma}(t))$ or 2D projections of Lissajous curves arranged in a Pipkin diagram (e.g. Fig. 4, Fig. 10). The LAOS characterization provides a more complete ñrheological fingerprintò which is especially important for understanding materials which exhibit elastic solid-like behavior at low strains, as this cannot be captured by steady flow curves.

We have considered various measures for identifying yield-like viscoplastic behavior as a function of the imposed LAOS deformation conditions, $\{\gamma_0, \omega\}$. Although the strain-stiffening ratio *S* and the shear-thickening ratio *T* accurately represent the measured intra-cycle

nonlinearities in the elastic and viscous properties of a complex fluid such as the oil-based drilling mud, they do not uniquely indicate yield stress behavior (Fig. 11).

We have introduced a new scalar parameter for identifying a plastic yield-like response under large amplitude oscillatory deformations, the perfect plastic dissipation parameter, $\Phi = E_d \big/ \left(E_d\right)_{pp}$, which uniquely identifies a plastic yield-like response as $\Phi \to 1$. Calculations with simple pseudoplastic and elastoplastic constitutive models, as well as experimental measurements, correspond to increasingly rectangular Lissajous curves. For regions of the Pipkin space in which $\Phi \to 1$, the dynamic yield stress in LAOS can be determined from the maximum value of the stress, $\sigma_{\max} = \sigma_Y$. Of the measures considered here, we conclude that Φ is the best choice for clearly identifying yield-like behavior in large amplitude oscillatory shear flow. The parameter Φ is straightforward to calculate, stable to dramatic nonlinear responses, and is associated uniquely with perfect plastic behavior.

For any material of interest, the relevant processing or in-use conditions can be related to the material response in an appropriate region of the Pipkin space $\{\gamma_0, \omega\}$. For such a set of conditions, the Lissajous curves and perfect plastic indicator, Φ, can be used in both a qualitative and quantitative fashion to identify if a specific fluid will appear (or feel, or process) like a perfect plastic material that yields at a given stress. We conclude that the LAOS protocol, and the parameter $\Phi = E_d \big/ \left(E_d\right)_{pp}$, can be used to provide more complete rheological fingerprints of an elastoviscoplastic material, and identify regimes within the shear deformation space $\{\gamma_0, \omega\}$ in which any material can be usefully considered to behave as a fluid with a critical or ñyieldò stress.

Acknowledgements

This work was supported in part by a gift from Procter & Gamble (Cincinnati, OH). R.H.E. gratefully acknowledges funding from the National Science Foundation Graduate Research Fellowship Program and the DARPA Chemical Robots program.

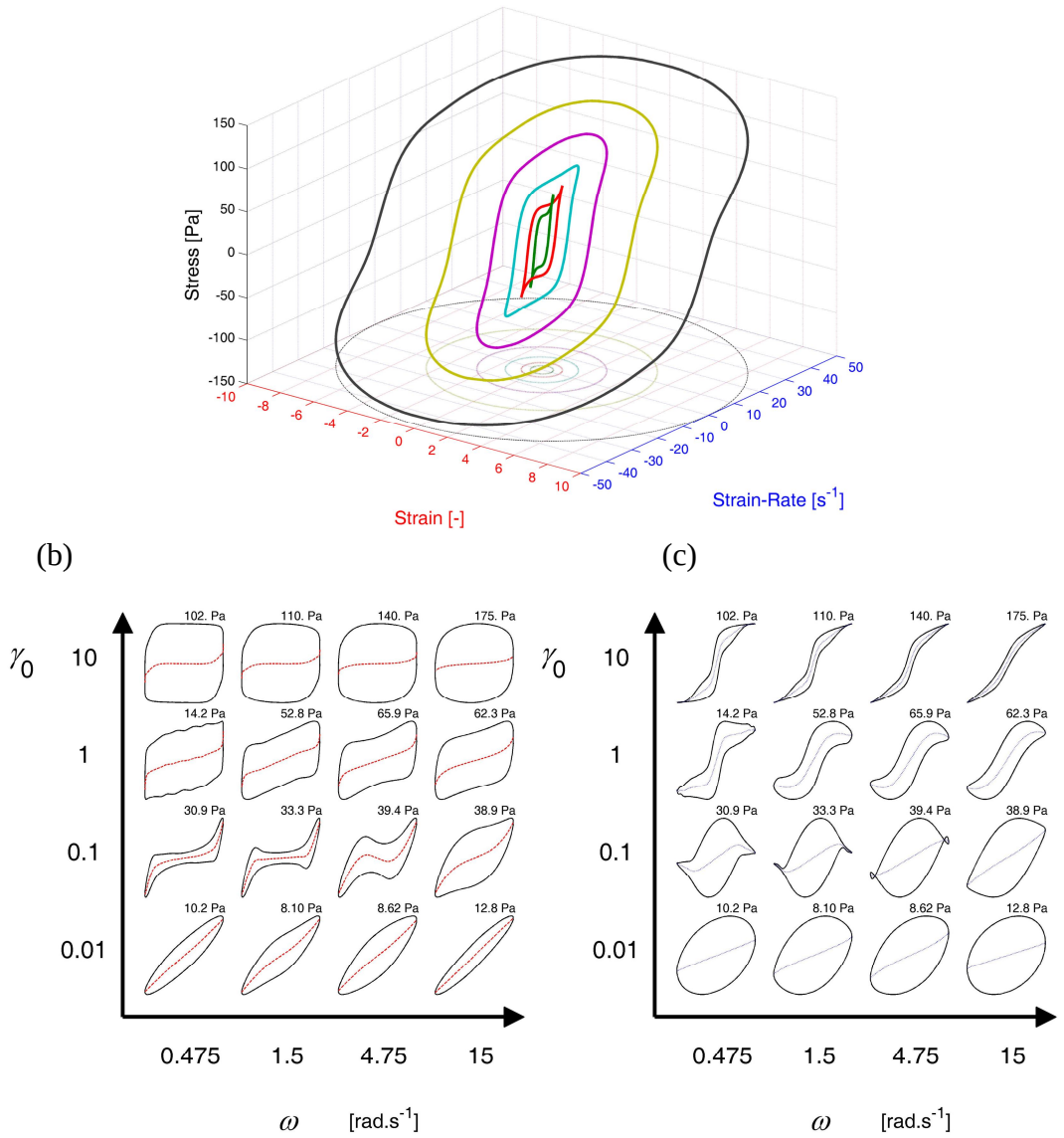

Fig. 10. Steady state Lissajous curves for the drilling fluid, shown for a selected range of strains and frequencies. (a) Un-normalized 3D curves for fixed ω=4.75 rad.s^{-1} and strain amplitudes $\gamma_0 = 0.562, 1, 1.78, 3.16, 5.62, 10$. (b,c) Normalized 2D projections of σ/σ_{max} arranged in a Pipkin space according to the input parameters $\{\gamma_0, \omega\}$ which generated each response curve. The maximum stress is shown above each curve. (b) individual plots of normalized stress (solid black lines) and elastic stress (dashed red lines) vs. strain, (c) individual plots of normalized stress (solid black lines) and viscous stress (dotted blue lines) vs. strain-rate.

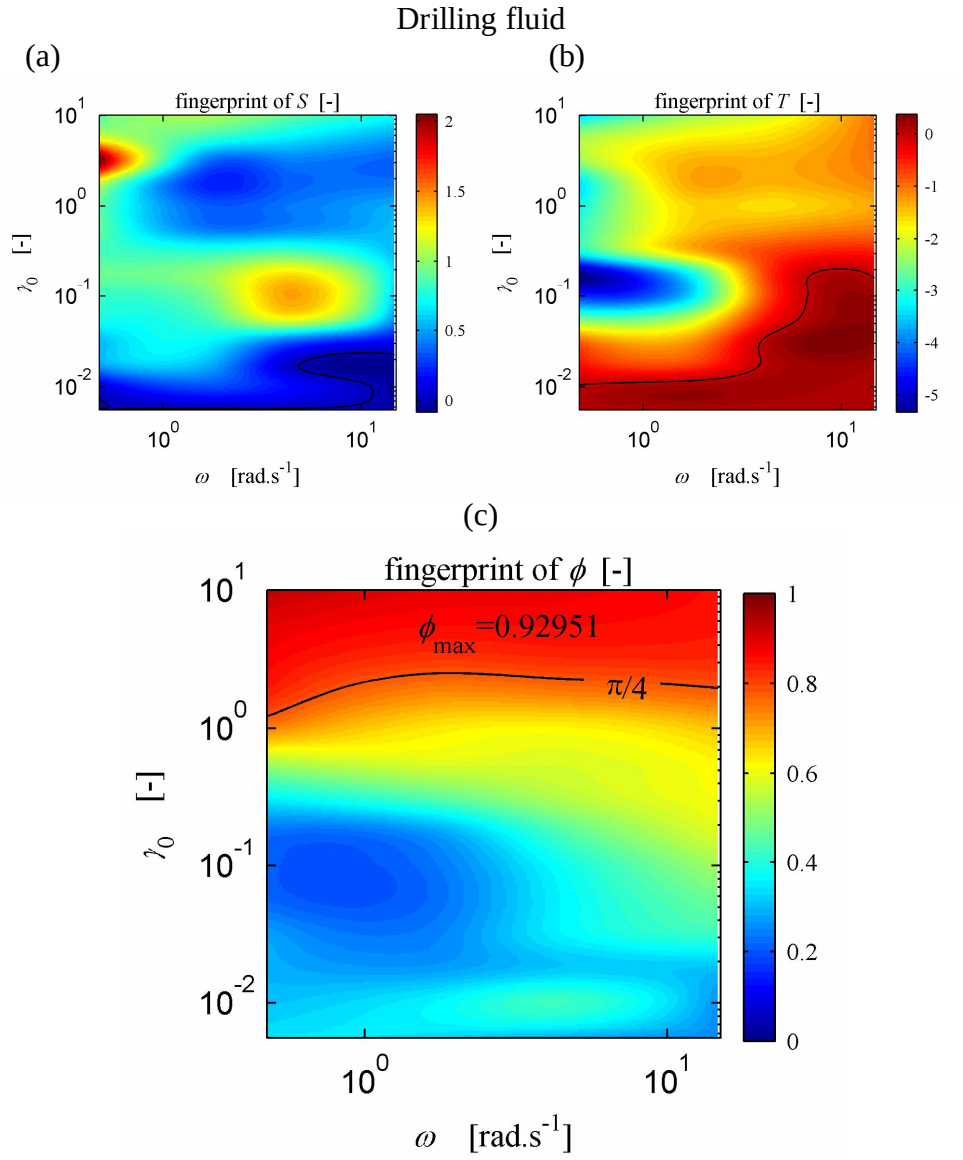

Fig. 11 Quantitative LAOS analysis of the drilling fluid. (a,b) Stiffening index and Thickening index, respectively, lines shown at S=0, T=0. (c) Perfect plastic dissipation ratio, ϕ, shown as contours in a Pipkin space. At small strain amplitude ϕ takes very small values indicated a predominantly elastic response, which at larger strain amplitude gives way to a predominantly viscous response and eventually a maximum dissipation ratio, $\phi_{max} = 0.93$, nearing the behavior of an idealized perfect plastic response.

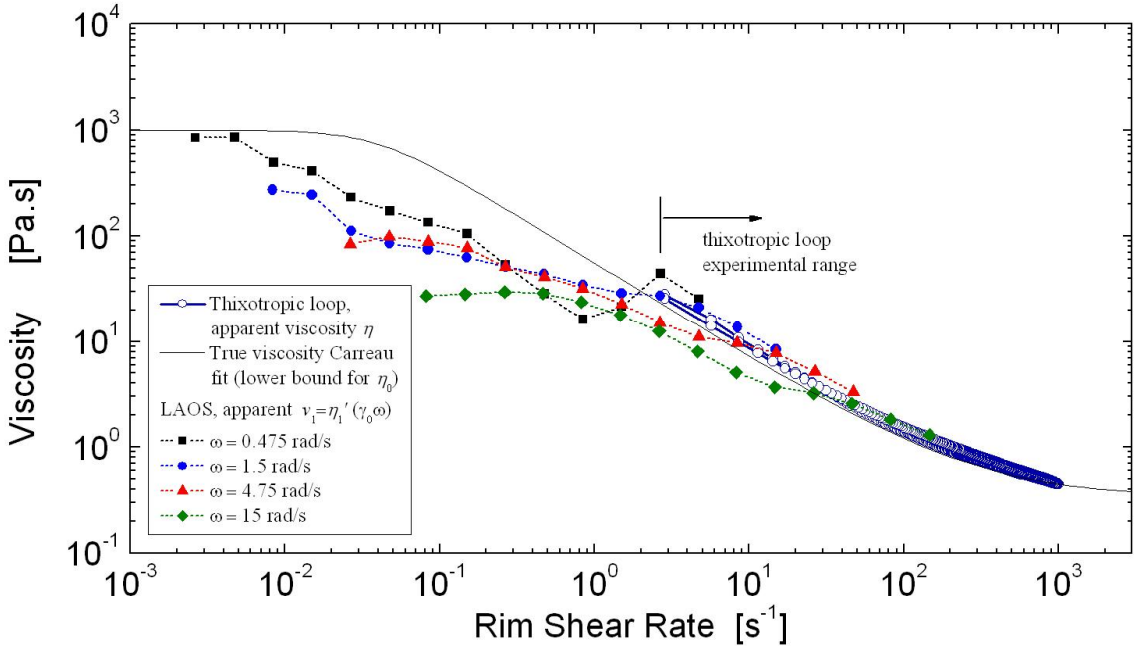

Fig. 12. First-harmonic dynamic viscosity $v_1(\dot{\gamma}_0) = \eta_1'(\dot{\gamma}_0)$ from LAOS tests (closed symbols) compared to the apparent shear viscosity $\eta(\dot{\gamma})$ from the thixotropic loop test (open circles). Good correspondence is found between the data at sufficiently large strain amplitudes $\gamma_0 \geq 3$, consistent with the Rutgers-Delaware rule. The viscosity at low shear-rates gives a lower bound for the Carreau model fitting parameter $\eta_0 = 1 \times 10^3$ Pa.s. The Carreau fit for $\eta_0 = 1 \times 10^3$ Pa.s, $\lambda = 53.5$ s, $n = 0.099$, and $\eta_\infty = 0.377$ Pa.s is given by the solid line.

Appendix

A.I Raw data from LAOS experiments

The full LAOS response of the xanthan gum, including transients, is shown in Fig. A1. The Lissajous curves of the raw measured stress vs. strain indicate an initial transient response which quickly settles into steady oscillatory orbits.

The drilling fluid LAOS response is shown in Fig. A2. Lissajous curves of apparent stress vs. rim shear-rate are arranged within a Pipkin space according to the LAOS input conditions $\{\gamma_0, \omega\}$. The startup transients settle into steady oscillations, which are used for the quantitative LAOS analysis presented here.

Both materials settle into steady oscillations which have the expected symmetry for shear-symmetric responses, i.e. any curve can be rotated by 180 degrees about an axis out of the page and result in the same steady oscillatory curve. This corresponds to the existence of only odd harmonics in the Chebyshev/Fourier representation, Eq. (6).

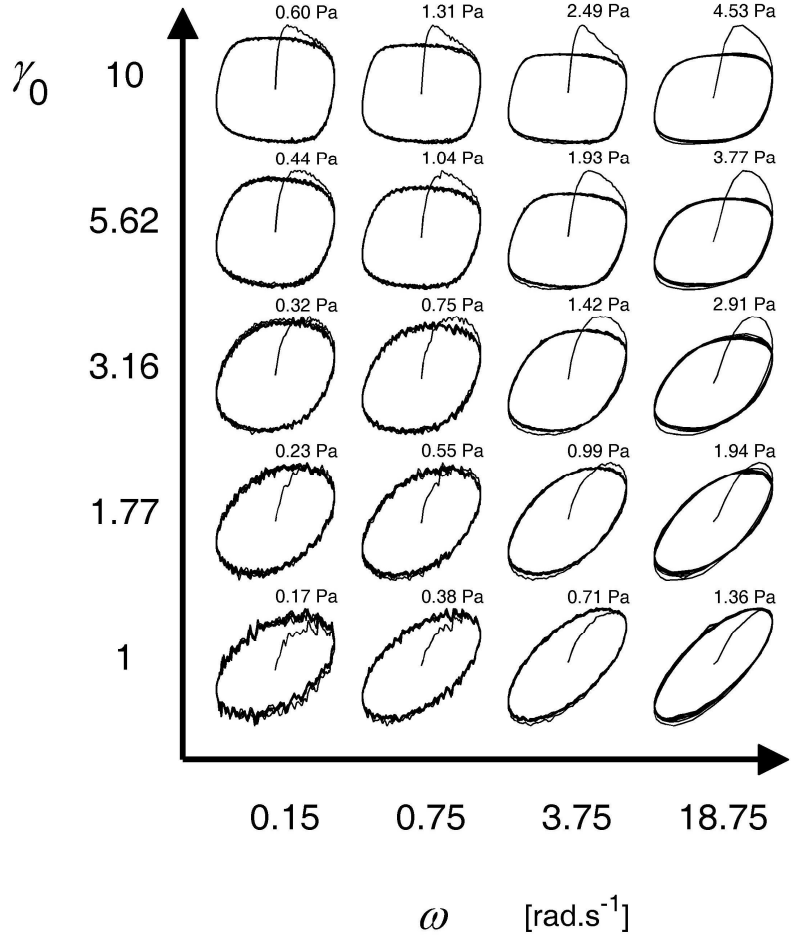

Fig. A1. Raw LAOS data for the xanthan gum solution (0.2wt% aqueous). Individual orbits are Lissajous curves of normalized stress vs. strain. The initial condition at the beginning of each test is $\gamma = 0$, $\sigma = 0$. Each individual plot is positioned within a Pipkin space according to the associated LAOS input parameters $\{\gamma_0, \omega\}$. The peak stress within each cycle (including the initial transient) is indicated above the individual curves.

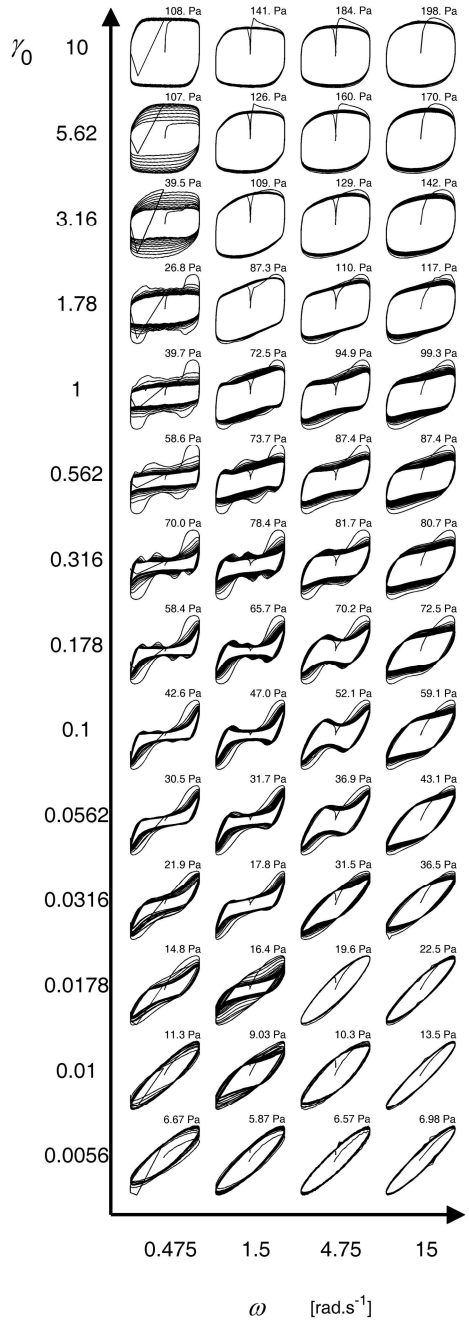

Fig. A2. Experimental LAOS data for the drilling fluid, including transients, shown as normalized Lissajous curves of stress vs. strain. The maximum absolute value of stress is shown above each curve. The test sequence consists of strain-amplitude sweeps (γ_0 = 0.0056 - 10) at constant frequency, in the order ω =(15, 4.75, 1.5, 0.475) rad.s^{-1}. The total number of cycles for each frequency is N=(19, 12, 20, 12) cycles for ω=(15, 4.75, 1.5, 0.475) rad.s^{-1}, respectively. The approach to the final periodic orbit can be identified visually. The data shown in Fig. 1 correspond to the test shown here at $\omega = 15$ rad.s^{-1}, $\gamma_0 = 3.16$. The final six steady oscillatory cycles are used for quantitative analysis of the limit cycle behavior.

A.II Interpolation method used for Pipkin space fingerprints

To improve visualization of trends and contour lines in the rheological fingerprints, the data are interpolated to produce smooth gradients, as in Fig.A3b. The figures presented here have been interpolated to include 100 points per decade in both frequency ω and strain-amplitude γ_0. The collection of experimental data occurs at discrete values within the Pipkin space of (ω,γ_0). For example, the drilling fluid data is spaced at 2 points per decade in frequency ω and 4 points per decade in strain-amplitude γ_0. The viscoelastic parameters corresponding to these discrete sampling points can be visualized by plots such as Fig.A3a. Color blocks are used for this plot, which are centered about the imposed values of (ω,γ_0). The width and height of the block area is determined by the spacing of the data. The finite width and height of each block increases the limits of the plot beyond where data was actually collected, since the blocks are centered over the corresponding (ω,γ_0) location. Only four strain-sweeps (at different fixed frequency) were used to create this fingerprint.

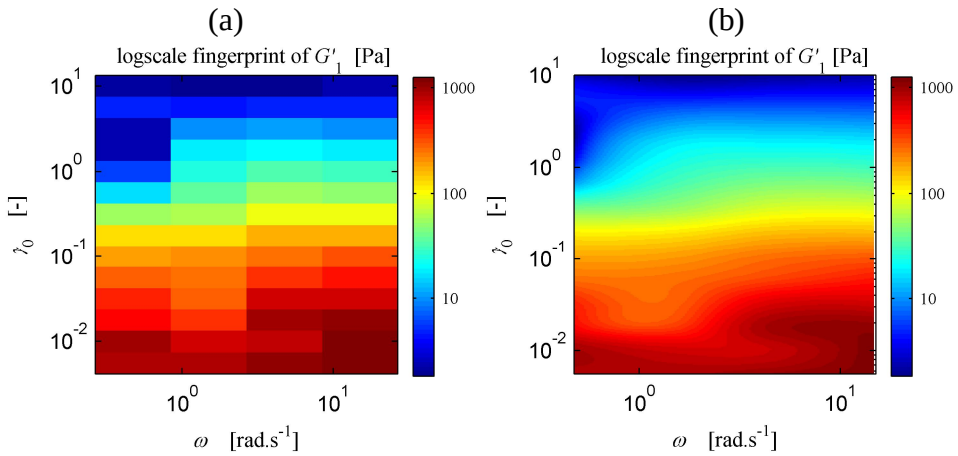

Fig. A3. Rheological fingerprint for the first-harmonic elastic modulus of the drilling fluid. Discrete experimental data points shown in (a) are interpolated to allow for smoothed gradients and contour lines within the Pipkin space (b).

References

A.P.I. (2009). Recommended Practice for Laboratory Testing of Drilling Fluids, American Petroleum Institute. **API RP 13I**

Atalik, K. and R. Keunings, "On the occurrence of even harmonics in the shear stress response of viscoelastic fluids in large amplitude oscillatory shear," Journal of Non-Newtonian Fluid Mechanics **122**(1-3), 107-116 (2004)

Barnes, H. A., "The yield stress - a review or `pi alpha nu tau alpha rho epsilon iota' - everything flows?," Journal of Non-Newtonian Fluid Mechanics **81**(1-2), 133-178 (1999)

Barnes, H. A. and K. Walters, "The Yield Stress Myth," Rheologica Acta **24**(4), 323-326 (1985)

Bird, R., R. Armstrong and O. Hassager, *Dynamics of Polymeric Liquids: Volume 1 Fluid Mechanics* (John Wiley & Sons, Inc, New York, 1987)

Bird, R. B., G. C. Dai and B. J. Yarusso, "The rheology and flow of viscoplastic materials," Reviews in Chemical Engineering. **1**(1), 1-70 (1983)

Brunn, P. O. and H. Asoud, "Analysis of shear rheometry of yield stress materials and apparent yield stress materials," Rheologica Acta **41**(6), 524-531 (2002)

Cho, K. S., K. H. Ahn and S. J. Lee, "A geometrical interpretation of large amplitude oscillatory shear response," Journal of Rheology **49**(3), 747-758 (2005)

Cross, M. M., "Rheology of non-Newtonian fluids: A new flow equation for pseudoplastic systems," Journal of Colloid Science **20**(5), 417-437 (1965)

Dealy, J. M. and K. F. Wissbrun, *Melt rheology and its role in plastics processing : theory and applications* (Van Nostrand Reinhold, New York, 1990)

Debbaut, B. and H. Burhin, "Large amplitude oscillatory shear and Fourier-transform rheology for a high-density polyethylene: Experiments and numerical simulation," Journal of Rheology **46**(5), 1155-1176 (2002)

Doraiswamy, D., A. N. Mujumdar, I. Tsao, A. N. Beris, S. C. Danforth and A. B. Metzner, "The Cox-Merz rule extended - a rheological model for concentrated suspensions and other materials with a yield stress," Journal of Rheology **35**(4), 647-685 (1991)

Ewoldt, R. H., A. E. Hosoi and G. H. McKinley, "New measures for characterizing nonlinear viscoelasticity in large amplitude oscillatory shear," Journal of Rheology **52**(6), 1427-1458 (2008)

Ewoldt, R. H. and G. H. McKinley, "Apparent self-intersection of Lissajous curves," Rheologica Acta (submitted in concert with this manuscript)

Ewoldt, R. H., P. Winter and G. H. McKinley (2007). MITlaos version 2.1 Beta for MATLAB. Cambridge, MA, self-published**:** MATLAB-based data analysis software for characterizing nonlinear viscoelastic responses to oscillatory shear strain.

Fischer, C., C. J. G. Plummer, V. Michaud, P. E. Bourban and J. A. E. Manson, "Pre- and post-transition behavior of shear-thickening fluids in oscillating shear," Rheologica Acta **46**(8), 1099-1108 (2007)

Ganeriwala, S. N. and C. A. Rotz, "Fourier-transform mechanical analysis for determining the nonlinear viscoelastic properties of polymers," Polymer Engineering and Science **27**(2), 165-178 (1987)

Graham, M. D., "Wall slip and the nonlinear dynamics of large-amplitude oscillatory shear flows," Journal of Rheology **39**(4), 697-712 (1995)

Harris, J. and K. Bogie, "The experimental analysis of non-linear waves in mechanical systems," Rheologica Acta **6**(1), 3-5 (1967)

Hyun, K., S. H. Kim, K. H. Ahn and S. J. Lee, "Large amplitude oscillatory shear as a way to classify the complex fluids," Journal of Non-Newtonian Fluid Mechanics **107**(1-3), 51-65 (2002)

Hyun, K. and M. Wilhelm, "Establishing a new mechanical nonlinear coefficient Q from FT-rheology: first investigation of entangled linear and comb polymer model systems," Macromolecules **42**(1), 411-422 (2009)

Jeyaseelan, R. S. and A. J. Giacomin, "Network theory for polymer solutions in large amplitude oscillatory shear," Journal of Non-Newtonian Fluid Mechanics **148**(1-3), 24-32 (2008)

Klein, C., H. W. Spiess, A. Calin, C. Balan and M. Wilhelm, "Separation of the nonlinear oscillatory response into a superposition of linear, strain hardening, strain softening, and wall slip response," Macromolecules **40**(12), 4250-4259 (2007)

Macosko, C. W., *Rheology : principles, measurements, and applications* (Wiley-VCH, New York, 1994) p.218

Macsporran, W. C. and R. P. Spiers, "The dynamic performance of the Weissenberg rheogoniometer. 2. large-amplitude oscillatory shearing - fundamental response," Rheologica Acta **21**(2), 193-200 (1982)

Macsporran, W. C. and R. P. Spiers, "The dynamic performance of the Weissenberg rheogoniometer. 3. large-amplitude oscillatory shearing - harmonic analysis," Rheologica Acta **23**(1), 90-97 (1984)

Maxey, J., "Thixotropy and yield stress behavior in drilling fluids," AADE 2007 Drilling Fluids Conference(AADE-07-NTCE-37) (2007)

Mitsoulis, E. (2007). Flows of viscoplastic materials: models and computations, in Rheology Reviews 2007. D. M. Binding, N. E. Hudson and R. Keunings. Glasgow, Universities Design & Print, Ch.

Mujumdar, A., A. N. Beris and A. B. Metzner, "Transient phenomena in thixotropic systems," Journal of Non-Newtonian Fluid Mechanics **102**(2), 157-178 (2002)

Papanastasiou, T. C., "Flows of materials with yield," Journal of Rheology **31**(5), 385-404 (1987)

Philippoff, W., "Vibrational measurements with large amplitudes," Transactions of the Society of Rheology **10**(1), 317-334 (1966)

Pipkin, A. C., *Lectures on viscoelasticity theory* (Springer, New York, 1972)

Rouyer, F., S. Cohen-Addad, R. Höhler, P. Sollich and S. M. Fielding, "The large amplitude oscillatory strain response of aqueous foam: Strain localization and full stress Fourier spectrum," European Physical Journal E **27**(3), 309-321 (2008)

Saramito, P., "A new constitutive equation for elastoviscoplastic fluid flows," Journal of Non-Newtonian Fluid Mechanics **145**(1), 1-14 (2007)

Stadler, F. J., A. Leygue, H. Burhin and C. Bailly,"The potential of large amplitude oscillatory shear to gain an insight into the long-chain branching structure of polymers," The 235th ACS National Meeting, New Orleans, LA, U.S.A.,Polymer Preprints ACS, **49,** 121-122 (2008)

Tee, T. T. and J. M. Dealy, "Nonlinear viscoelasticity of polymer melts," Transactions of the Society of Rheology **19**(4), 595-615 (1975)

Ugural, A. C. and S. K. Fenster, *Advanced strength and applied elasticity* (Prentice Hall, Upper Saddle River, N.J., 2003)

van Dusschoten, D. and M. Wilhelm, "Increased torque transducer sensitivity via oversampling," Rheologica Acta **40**(4), 395-399 (2001)
Wilhelm, M., "Fourier-Transform rheology," Macromolecular Materials and Engineering **287**(2), 83-105 (2002)
Wilhelm, M., P. Reinheimer and M. Ortseifer, "High sensitivity Fourier-transform rheology," Rheologica Acta **38**(4), 349-356 (1999)
Yoshimura, A. S. and R. K. Prudhomme, "Response of an elastic Bingham fluid to oscillatory shear," Rheologica Acta **26**(5), 428-436 (1987)
Yoshimura, A. S. and R. K. Prudhomme, "Wall slip effects on dynamic oscillatory measurements," Journal of Rheology **32**(6), 575-584 (1988)
Yu, W., P. Wang and C. Zhou, "General stress decomposition in nonlinear oscillatory shear flow," Journal of Rheology **53**(1), 215-238 (2009)